ABSTRACT

CHAN, RYAN NICHOLAS. Fracture Properties of Yttria-Stabilized Zirconia (YSZ) Thin-Film Modified Constructs. (Under the direction of Jeffrey R Piascik and Ronald O Scattergood).

Dental restoration technologies allow for patients to return function, integrity, and aesthetics to damaged or missing teeth. Recent studies on the link between oral and general health, has led to a shift in focus towards oral-health-related quality of life. Within the United States alone, an ageing population has driven demand for health systems and technology. Similarly, increasing global life expectancy and economic development has led to a strong focus on personal heath/wellness. With recent studies indicating links between oral and general health, much attention has been spent on improvements to dental materials and technologies.

All-ceramic materials, such as porcelain and partially-stabilized zirconia (PSZ), have made strong headways into recent use as dental restorations, where aesthetic properties are highly coveted. Particularly, recent attention has been given to dental ceramics due to the relative ease in which their appearance can be matched to natural teeth. However when compared to their metal and metal-ceramic hybrid counterparts, ceramic restorations are disadvantaged by their reduced capacity to resist crack propagation. As a result, strengthening properties are of particular interest in all-ceramic materials where common preparation techniques involve surface roughening by abrasion or etching to increase the bonding surface area of a construct. However, these roughening techniques may also impart surface flaws, resulting in premature failure of a restoration. Under tension, surface flaws

may act as potential stress-concentration and crack-initiation sites, allowing cracks to propagate more easily, thereby limiting the strength of ceramics.

The corrosion and wear resistance properties of ceramics, such as partially-stabilized zirconia (PSZ), along with the unique microstructures achievable by thin-film deposition, have made ceramic thin-films particularly appealing for use as protective coatings. Furthermore, it has been shown that the application of thin-films to a dental ceramic can result in increased flexural strength. Recent investigations have shown an improvement in fracture strength in dental ceramics through sputter deposition of yttria-stabilized zirconia (YSZ) thin-films. It is hypothesized that films with differing microstructure and compressive film stress will further enhance a construct's fracture strength.

Here, feldspathic porcelain substrates were cut from commercially available porcelain (ProCAD, Ivoclar-Vivadent) blocks and wet-polished through 1200-grit using SiC abrasive. Utilizing radio frequency (r.f.) magnetron sputtering, yttria-stabilized zirconia films (2-3μm) were deposited with varying deposition parameters. Film and flaw properties were characterized by optical microscopy, scanning electron microscopy (SEM), x-ray diffraction (XRD), and wafer bow analysis. Flexural strength was determined by ring-on-ring biaxial flexure, and three-point bending. Fracture toughness values were calculated from flaw size and fracture strength. Fractography and Weibull analysis was then conducted to supplement fracture behavior observations and to develop a mechanistic understanding of observed trends.

By depositing PSZ films of varying microstructures and film stresses, this study aims to show a further increase in mechanical properties in PSZ-altered constructs. Data show improvements in fracture strength of up to 55% over unmodified specimens. XRD analysis shows that films deposited with higher substrate bias displayed a high %monoclinic volume fraction (19%) compared to non-biased deposited films (87%), and resulted in increased film stresses and modified YSZ microstructures. SEM analysis shows critical flaw sizes of 63$\pm$1µm leading to fracture toughness improvements of 55% over unmodified samples. Data supports surface modification of dental ceramics with YSZ thin film coatings to improve fracture strength. Increase in construct strength was attributed to increase in compressive film stresses and modified YSZ microstructures. It is believed that this surface modification may lead to significant improvements and overall reliability of all-ceramic dental restorations. This work also aims to propose a simplistic model of strengthening mechanisms to assist in predicting fracture behavior improvements.

Fracture Properties of Yttria-Stabilized Zirconia (YSZ) Thin-Film Modified Constructs

by
Ryan Nicholas Chan

A dissertation submitted to the Graduate Faculty of
North Carolina State University
in partial fulfillment of the
requirements for the degree of
Doctor of Philosophy

Materials Science and Engineering

Raleigh, North Carolina

2013

APPROVED BY:

Jeffrey R Piascik Committee Chair Co-Chair	Ronald O Scattergood Committee Chair Co-Chair
Korukonda Murty	Mike Rigsbee

DEDICATION

To my parents, Frank and Lily Chan, who have made all my successes possible.

BIOGRAPHY

Ryan Chan was born to parents Frank and Lily Chan in upstate New York. In his early years he was lovingly raised alongside younger brother Alex Chan. Since 1995, Ryan’s family has resided in the Triangle area where he quickly took a keen interest in music and the sciences. His interests led him towards accumulating musical and academic honors which were continued aspirations upon entering college.

Ryan entered the Materials Science and Engineering (MSE) program at NC State University in the fall of 2005 where he quickly rooted himself in the university bands as well as in undergraduate research. Throughout his undergraduate studies, Ryan was fortunate to work with professors Ronald Scattergood, Carl Koch and then-graduate student Kristopher Darling. Here he had the early opportunity to gain valuable research experience by working on stabilizing grains in nanocrystalline alloys. These mentors helped set the framework for Ryan’s research experience and more importantly, helped to highlight his desired career path. Meanwhile, Ryan’s musical pursuits allowed him to be appointed into multiple leadership positions by the University’s Director of Bands, Dr. Paul Garcia. Through various musical ensembles, Ryan had the opportunity to travel with these ensembles to numerous venues across the globe. These venues included an array of athletic stadiums, and were punctuated by performances in the Sydney opera house and they Dublin St. Patrick’s Day Parade.

In the summer of his Junior year, Ryan gained the opportunity to intern at Corning Inc. where he studied the effect of damage accumulation in advanced substrate systems. Here he gained valuable industrial R&D experience by working closely with Dr. Sujanto Widjaja and other failure analysis experts in the Fundamental Research Branch at Corning's Sullivan Park R&D Center. In Ryan's senior year, he had the opportunity to work with an outstanding group of MSE students on a senior design project funded by Northrop Grumman. This project allowed him to explore novel thin film thermocouple technologies for harsh conditions. The skills gained from these projects would set the stage for an early start on Ryan's graduate studies.

Ryan received his Bachelor of Science in the spring of 2009 and promptly began graduate work the following summer thanks to an opportunity provided by Jeff Piascik and Brian Stoner at RTI International. While working at RTI, Ryan's project utilized aspects from all of his undergraduate studies and required development of much refined analytical and critical thinking skills. Thanks to the outstanding support of his advisors and co-workers, Ryan was able to travel to numerous conferences and events across the country to share and discuss his work with key experts in his field. Ryan looks forward to the opportunity to be a co-founder of Tethis Inc. Thanks to the valuable experience gained throughout Ryan's collegiate career, the future is open and full of possibilities.

ACKNOWLEDGEMENTS

The work contained here would not have been possible without the outstanding support and direction of Dr. Jeffrey Piascik. His patience and guidance has directly led to my proficiency in the field. Most of all, I'd especially like to thank Jeff for teaching me the value of a simple slide deck. This skill has allowed me to communicate with a versatility that will be invaluable throughout my career. Much credit is given also to Dr. Ronald Scattergood and Dr. Brian Stoner for helping me sift through the years or endless revisions of papers, plans, and presentations. Our colleagues, Dr. Jeffrey Thompson and Dr. Robert Smith at Nova Southeastern University have also provided valuable advice, which led towards the development of much of the fractography work discussed here.

While working at RTI, I have been fortunate to have incredible coworkers who were always willing to donate their time, skills, and comments. To them goes my gratitude: To Dana Fox for teaching me more than I ever thought I could learn about using an SEM. To Enzo Cellini, Dan Patterson, Mike Bucholz for helping me maintain the finicky, yet essential CVC system required for this work. To Doug Roberson for the amusing, yet informative discussions about how the world "really" works.

I would also like to recognize my incredible friends who have persisted with me throughout the years: Thanks to the group from suite 503: Matt, Jit, Trenton, Jason, and Taylor for always keeping me grounded, for better or for worse. To Annie for providing order to my life, sometimes despite my strong opposition. And to my band friends for showing me that every now and again, a break can be helpful. Most of all, I'd like to thank my family. My brother Alex and my parents Frank and Lily have provided an encouraging atmosphere in all aspects of my life which has allowed me notch many accomplishments with hopefully many more to come.

TABLE OF CONTENTS

LIST OF TABLES

LIST OF FIGURES

LIST OF ABBREVIATIONS

CTE	Coefficient of Thermal Expansion
Al_2O_3	Alumina
ZrO_2	Zirconia
SiC	Silicon Carbide
m-ZrO_2	Monoclinic Zirconia
t-ZrO_2	Tetragonal Zirconia
c-ZrO_2	Cubic Zirconia
Si-O-Si	Silicon-Oxygen-Silicon bonding structure in glass ceramics
FE-SEM	Field Emission Scanning Electron Microscopy
PSZ	Partially Stabilized Zirconia
YSZ	Yttria Stabilized Zirconia
PVD	Plasma Vapor Deposition
R.F.	Radio Frequency
XRD	X-Ray Diffraction
SEM	Scanning Electron Microscopy
ASTM	American Society for Testing and Materials

LIST OF SYMBOLS

W	Watt
N	Newton
μm	Micron
°C	Degrees Celsius
T	Temperature
E	Elastic modulus
α	Coefficient of thermal expansion
σ	Stress
γ	Surface Energy
$I_{M(111)}$	Intensity of the (111) monoclinic peak
$I_{T(111)}$	Intensity of the (111) tetragonal peak
Ar	Argon
Zr	Zirconium
O2	Molecular Oxygen

CHAPTER 1: INTRODUCTION TO DENTAL MATERIALS & STATEMENT OF PURPOSE

Structure-property relationships are studied as a means for understanding fundamental mechanistic principles within a system. In modern times, these relationships have been used to optimize and/or advance the boundaries of numerous technological systems. In the biomedical field alone, these materials science principles have driven countless significant improvements to technologies ranging from biocompatible prostheses, to medical devices, to diagnostic and therapeutic tools, to regenerative tissue systems. Increasing global life expectancy and economic development has led to a strong shift in focus towards sustainable health and wellness. Within the United States, an ageing population has driven the demand for these improved health systems and technologies.

Recent studies on the link between oral and general health, has led to a shift in focus towards oral-health-related quality of life.[1] Studies have shown that losing the ability to chew can have detrimental impacts on nutritional status.[2] Additionally, a recent report by Frost and Sullivan lists the ageing baby boomer population in developed nations and societal pressures as the two primary market drivers for advancement in dental materials.[3] Growth in general expectations of personal appearance and aesthetic smiles has driven a market where significant percentages of disposable incomes are spent on dental restoration procedures. Due to the large demand for dental procedures, the global dental implants and prosthetics market was estimated to be $6.8 billion in 2011 and is expected to grow to over $10.5 billion by 2016.[4]

Many of the recent advances in biotechnology can be directly attributed to materials science and its governing principals. These technologies allow for patients to return function, integrity, and aesthetics to damaged body parts with ever increasing speed and reliability. However, materials selection for the oral environment presents unique challenges that are not generally found throughout the rest of the human body.[5] In terms of mechanical properties, dental restorations must withstand high contact stresses as well as the typical cyclic stresses associated with chewing. Furthermore, materials must be able to withstand thermal expansion differences ranging from the exposure to ice to hot foods/liquids as well as a wide range of pH values.

Of the primary classes of materials, ceramics are generally favored when chemical stability, high compressive strength, optical, and/or refractory properties are required. In biomaterials applications, bioceramics are typically used to replace and repair hard connective tissues.[6] Therefore wear resistance and osteointegration properties of ceramics in biological applications such as articulating surfaces (joints), prosthodontics, and bone growth/repair drive materials selection decisions. Compared to their, metal counterparts, ceramics rarely illicit an allergic response, or release ionic species into surrounding tissues.[7]

The corrosion and wear resistance properties alone make ceramics a prime candidate for dental restorations. As previously mentioned, aesthetics act as an additional driving force in dental procedure decision making.[8-10] The ability to precisely match color, shading, and translucency of ceramics with surrounding teeth has only further solidified its expansion in dentistry. However in applications of ceramic materials can be inhibited by inferior mechanical properties compared to other materials classes. Fracture toughness values, a materials property governing the ease of crack expansion and propagation, generally indicate weak crack resistance for ceramics. Despite a tolerance for high compressive stresses, the potential for catastrophic brittle failure under tensile loading has limited the use of ceramics in more demanding load bearing applications.

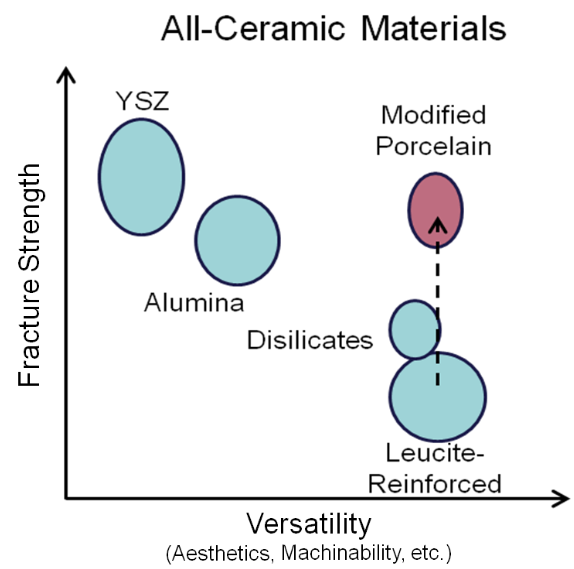

Figure 1.1: Various dental ceramics arranged by fracture strength and versatility illustrates the trade-offs made during materials selection of dental ceramics.

However when applicable, informed materials selection may allow for improved mechanical reliability for a given application. Ceramic materials used in dental restorations typically fall into three different categories ranked in ascending order of fracture strength[7]:

1) Glass ceramics: Feldspathic Porcelain [~60-70MPa]

2) Glass ceramics with fillers: Leucite-reinforced [~120MPa], Lithium Disilicates [~360MPa], Glass-Infiltrated [350-650MPa]
3) Glass-Free, Polycrystalline Ceramics: Alumina [600-700MPa], Zirconia [~1120MPa]

As shown in figure 1.1, there exists a tradeoff between improved fracture behavior and system versatility. Of the dental restorative procedures (inlays, onlays, crowns, bridges, and veneers), while a material with increased fracture strength would offer increased reliability, a more versatile material would be of wider use in dental restorative procedures to successfully restore structure of a decayed or missing tooth.[7]

Traditionally, translucent glass ceramics (feldspathic porcelain) have been used for numerous dental restoration applications. However this material lacked the mechanical properties needed for more intensive restorations such as implants. As such, porcelain is now limited to veneer or coating applications. Conversely, alumina and zirconia provide greatly improved fracture strengths over porcelain systems. However these polycrystalline ceramics typically require an outer porcelain veneer layer to provide a more aesthetic, translucent quality to the restoration. As an alternative, and due to the versatility of glass-ceramics, much work has been conducted to improve the fracture strength of glass-ceramic systems using fillers and/or more mechanically stable additives.

Restorative procedures can involve using fillings, mounting a prefabricated component to existing tooth structure, or in the case of more severe restorations, the procedure may require a surgical implant to anchor prosthetic structures.[5] Once a material is selected, restorations are then processed in one of three primary methods:

1) Powder/liquid fabrication
2) Pressing or molding
3) CAD/CAM subtractive or additive processing

The introduction of computer-aided design and computer-aided manufacturing (CAD/CAM) technologies to dentistry has significantly improved procedure time to allow for same-day generation of dental restoration products. As a result, CAD/CAM technologies are largely credited towards the recent advancements in ceramic dentistry, leading to expanded access and demand for all-ceramic restorations. According to a 2001 report by the World Health Organization (WHO) on the status of global oral health, ceramic restorations provide an aesthetic and sustainable alternative to traditional metal components; however there remain concerns about the longevity of ceramic restorations, in part due to their mechanical properties.[11]

Furthermore, clinical dental restorations are typically etched or air abraded on the tissue-side of the restoration to roughen surfaces for improved adhesion. These clinical procedures increase surface area for improved bonding to dental resins; however, these techniques simultaneously induce large surface flaws, increasing the number of potential flaw initiation sites and the chance of premature failure.[12-14] Fracture strength of brittle materials, such as dental ceramics, are typically characterized by an elliptical, initial flaw surrounded by a larger, elliptical area that designates the flaw size.[15-16] According to ceramic fracture toughness principles, for a given material's system, a component's strength is dictated by size and geometry of these critical flaws.

Strength improvements for dental ceramics have been demonstrated through various surface modification methods; such as, flaw modification, heat treatments, and coatings. Fundamentally, by controlling surface finishing techniques, fracture toughness can be enhanced through modification of surface flaws, resulting in reduced stress concentration in the local area of a critical flaw and increasing overall strength of a sample.[12. 15] Compressive stress gradients can also be introduced to a sample through thermal processing, where a surface is cooled at a faster rate than the interior of a sample, resulting in a compressive surface.[17-18] Composition gradients and ion implantation techniques have also been used to induce strain into the crystal lattice, resulting in compressive stresses on a sample surface.[19] These stress-modification mechanisms require crack expansion (or increased tensile stresses), to overcome the induced compressive stresses on the surface of a sample. As a result, crack propagation is inhibited, resulting in increased fracture toughness.

Thin film coatings have been employed to strengthen substrates; first through critical flaw modification and secondly through inducing compressive surfaces stresses.[20-21] Ruddell et al. has shown improvements in fracture strength of up to 19% by coating ceramic substrates with less than 10μm of sputtered metallic thin films.[20, 22] Earlier work reported increases in strength of up to 32% by using a multilayer film (10 μm) structure consisting of alternating layers of yttria-stabilized zirconia (YSZ) (1 μm) and parylene (1 μm) to induce crack deflection.[23] Additionally, it was determined that a 2-3 μm thick YSZ thin film sputtered on porcelain substrates provide the maximum benefit for increased construct fracture strength.[21]

This work aims to study the mechanical properties of PSZ-altered ceramic constructs as a viable method for improving the longevity and reliability of all-ceramic dental restorations. Applying a compressive, thin-film coating to all-ceramic substrates, is expected to provide strength advantages over current, clinical preparation methods by altering fracture behaviors in a positive manner. Furthermore, by developing associated models for thin-film-ceramic constructs this work aims to provide quantitative analysis of compressive thin-film forces, based on associated strengthening mechanisms.

CHAPTER 2: LITERATURE REVIEW & FUNDAMENTALS

Unlike ductile materials such as metals or polymers, ceramics have a tendency to fail many orders of magnitude below their theoretical fracture strength. It was theorized by Griffith that the fracture strength discrepancies could be explained by the presence of microscopic flaws distributed throughout the material.[24] These flaws generally arise from microscopic imperfections or defects, distributed throughout a given sample. Under an applied load, these defects act as stress amplification and crack nucleation sites which eventually lead to catastrophic, brittle failure. The initiation site of specimen failure is known as the critical flaw.

Griffith explained this behavior in glass systems by introducing a critical flaw to the surface of samples to normalize the fracture origin. He showed that in brittle systems, the following relation held true:

$$\sigma_f \sqrt{a} \approx C \qquad \text{Eq. [2.1]}$$

Where σ_f is fracture stress, a is flaw size and the product of the two values was approximately equal to a constant value. To elaborate on this relation in terms of energy, it was further modified under the assumption that under an applied load, crack propagation occurs, causing the creation of new surfaces.[24] The elastic energy is then converted to surface energy by the equation below:

$$C = \sqrt{\frac{2 \cdot E \cdot \gamma}{\pi}} \qquad \text{Eq. [2.2]}$$

Where C represents a constant value at a given fracture stress and flaw size, E represents elastic modulus, and γ represents surface energy density,

This theory was later modified by Irwin to account for the dissipation of energy through a plastic zone in non-brittle failure.[25] After modification, the equation then reads as:

$$\sigma_f\sqrt{a} = \sqrt{\frac{E \cdot G}{\pi}} \qquad \text{Eq. [2.3]}$$

Where σ_f is fracture stress, a is flaw size, E is elastic modulus, and G is the total energy including surface energy and dissipation from other sources (plastic failure). This equation was later further modified to create a parameter called stress intensity, which is defined in equation 2.4 below:[26]

$$K_I = \sigma\sqrt{\pi \cdot c} \qquad \text{Eq. [2.4]}$$

Where K_I is stress intensity [$MPa \cdot m^{1/2}$], σ is the applied stress [MPa], and c [m] is the flaw size. A materials parameter known as critical stress intensity or fracture toughness can also be defined by the following equation:

$$K_{Ic} = \sqrt{2 \cdot \gamma \cdot Y} \qquad \text{Eq. [2.5]}$$

Where K_{Ic} is the fracture toughness, γ is the surface energy of the material, and Y is the Young’s modulus. The condition for fracture is then defined as when the stress intensity exceeds the fracture toughness of the material as showing in Eq. 2.6.

$$K_I \geq K_{Ic} \qquad \text{Eq. [2.6]}$$

Experimentally, fracture toughness can be measured using the equation below:

$$K_{IC} = Y\sigma_f\sqrt{a} \qquad [2.7$$

Where K_{IC} is the mode I critical stress intensity factor (fracture toughness) [$MPa\sqrt{m}$], Y is a geometry-dependent shape factor, σ_f is fracture stress [MPa], and a is the radius of the critical flaw [m].[27]

2.1 Bulk Ceramic Toughening Mechanisms

An ongoing goal of materials science and engineering has been to push the limits of materials towards applications in increasingly demanding and hostile applications. Although ceramic materials are inherently brittle, increasing the fracture toughness of materials systems has driven multiple toughening mechanisms (Figure 2.1) to be harnessed to improve the usefulness of ceramics. In a variety of applications, these toughening mechanisms work concurrently to fracture mechanics principles by increasing the energy required to propagate a crack.

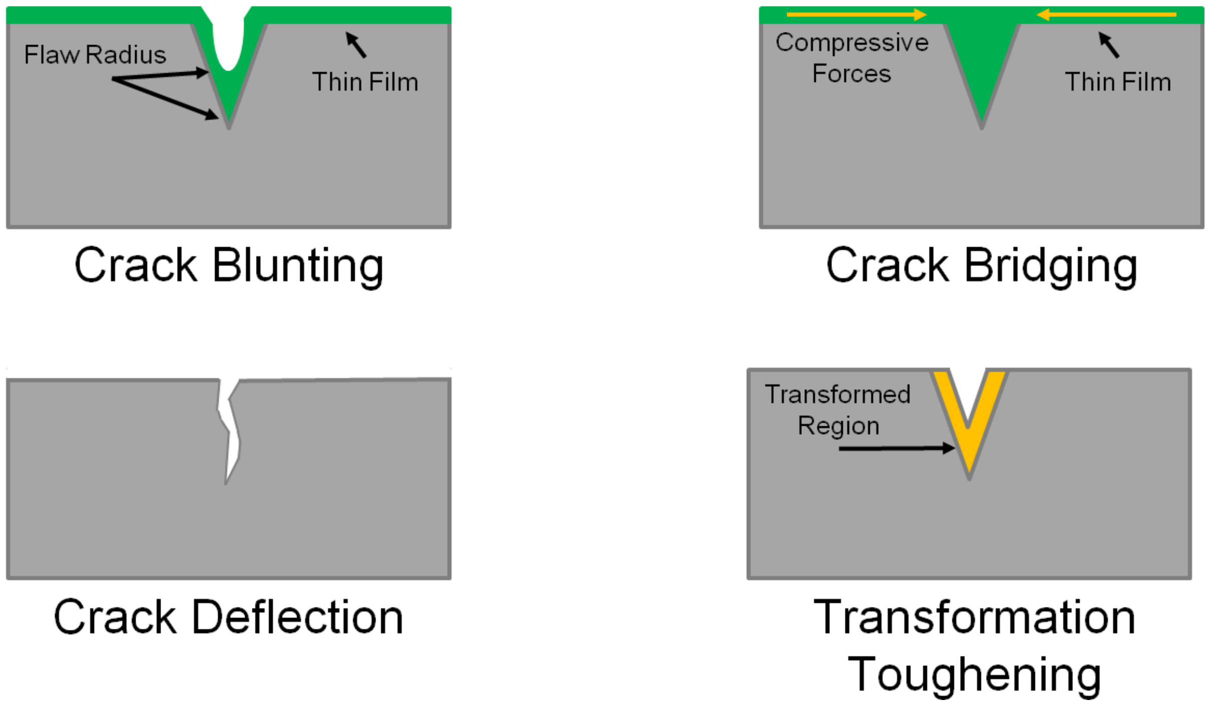

Figure 2.1: Ceramic toughening mechanisms are derived from an increased energy requirement for crack propagations by way of modifying critical flaws and their associated crack paths.

One toughening mechanism, known as crack deflection, results from an increased traveled distance by a propagating crack upon failure. By requiring the formation of new surfaces over larger distances, energy requirements for fracture are greatly increased.[28] Furthermore, by altering, or modulating the angle of crack propagation, the direction of propagation will no longer be always normal to the direction of applied stress. This variation in crack propagation angle relative to the crack plane causes a reduced magnitude of stress in the direction of crack propagation. These principles are most apparent in the case of polycrystalline materials relative to their single crystal counterparts. For example, in the case of alumina (Al_2O_3), fracture toughness for a single crystal system is approximately 2.2 $MPa{\cdot}m^{1/2}$ whereas polycrystalline alumina has a fracture toughness of approximately 4 $MPa{\cdot}m^{1/2}$. The difference in fracture toughness values in attributed to intergranular fracture. This principle has been applied to many materials systems including a few general examples below:[29-32]

a) Using particles, inclusions, or agglomerates of second phases dispersed through a bulk matrix to deflect of bifurcate propagating cracks.

b) Using porosity or controlling defects generated during processing to deflect or channel crack propagation.

c) Using rods or fibers to induce delamination and/or severe disruptions to the angle of crack propagation.

In the above example, a porous sample generally has a reduced fracture behavior relative to its non-porous counterpart. However for a given porosity, fracture toughness can be improved using a supplementary mechanism known as crack-tip blunting. In this toughening mechanism, stress concentration can be reduced due to an increased radius of curvature in the proximity of an advancing crack tip.[33] This mechanism was experimentally demonstrated by showing increased fracture toughness values for larger pore sizes of equivalent geometry. Crack tip blunting is also demonstrated in applications where surface finishing such as polishing or coatings can be used to increase the radius of curvature at the crack front of a critical flaw, resulting in improved fracture behaviors.

An additional toughening mechanism, termed crack bridging, employs reinforcing phases or components to counteract tensile forces imparted on a critical flaw. Generally fibers or fibrous grains can be used to bridge a propagating crack front, which provides support to an advancing crack. This mechanism effectively results in the distribution of an applied load over the additional bridges, which results in a reduction in stress intensity at the crack propagation front. Additionally, these bridges may have increased fracture toughness relative to the surrounding matrix and/or may have residual compressive stresses. A higher applied load is then required to fracture or debond these bridges. This mechanism is prevalent in composite systems where a strong or directionally-aligned, fibrous material is used to reinforce a weaker surrounding matrix.[34] Tempered glass systems employ a modified version of the crack bridging mechanism by imparting high compressive stresses into the outer surfaces of a component. These residual surfaces stresses require applied loads to overcome the inherent strength of the material plus the additional surface stresses in order to propagate surface flaws to failure.

2.2 Transformation Toughening: The Zirconia System

Another prevalent toughening mechanism, called transformation toughening, is found in Zirconia (ZrO_2) and Alumina (Al_2O_3) materials systems. This toughening mechanism takes advantage of diffusionless phase transformations observed in some materials systems to apply compressive stresses on propagating cracks. In particular, partially-stabilized zirconia (PSZ) is an attractive material due to its high fracture toughness relative to other ceramic materials (6-10 MPa·$m^{1/2}$); which is attributed to phase transformation and microcrack toughening mechanisms.[26, 35-39]

Transformation toughening is particularly apparent in PSZ, where dopants such as CaO, MgO, Y_2O_3, and/or CeO_2 can be used to stabilize high-temperature phases of zirconia at room temperature.[40] At room temperature and ambient pressures, undoped zirconia (ZrO_2) exists with a monoclinic crystal structure.[35] As shown in Figure 2.2, increasing temperatures causes zirconia to undergo tetragonal (t-ZrO_2) and cubic (c-ZrO_2) phase changes at intermediate (~1000°C) and high (~2370°C) temperatures, respectively.[35]

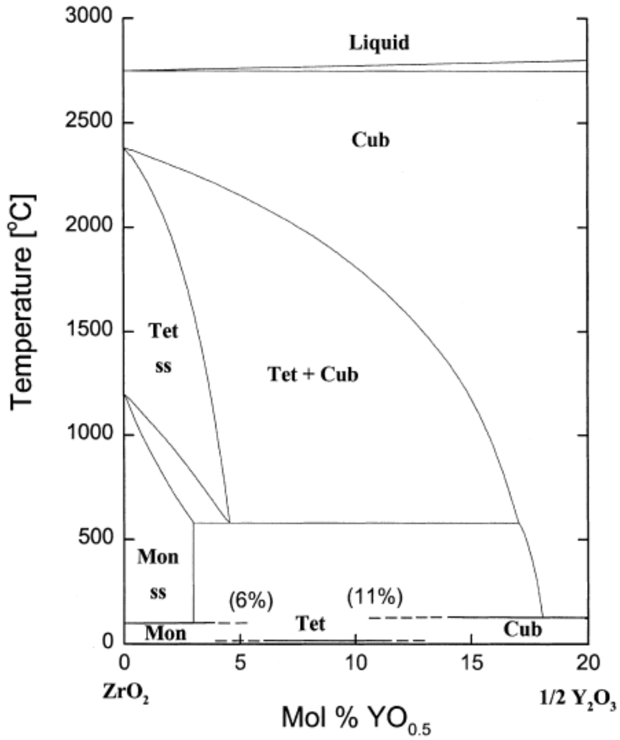

Figure 2.2: Phase diagram for zirconium oxide doped with yttrium oxide [41].

In particular, the tetragonal to monoclinic (*t* → *m*) phase transformation has received considerable attention due to its diffusionless character, similar to that of martensitic steel.[35] In the case of yttrium oxide (Y_2O_3), doping concentrations of up to ~9wt% Y_2O_3 are used. At concentrations above 3wt%, the tetragonal phase is favored at room temperatures, whereas the monoclinic phase is favored at concentrations less than or equal to 3%.[41] For 3% Y_2O_3, larger Y^{3+} ions are substituted for Zr^{4+} ions, where charge neutrality dictates the presence of oxygen vacancies.[35] Additionally, the increased ionic radii (0.96Å vs. 0.82Å) of Y^{3+} imparts sufficient strain on the surrounding lattice to allow the tetragonal phase of zirconia to exist in a metastable state at room temperature.[35]

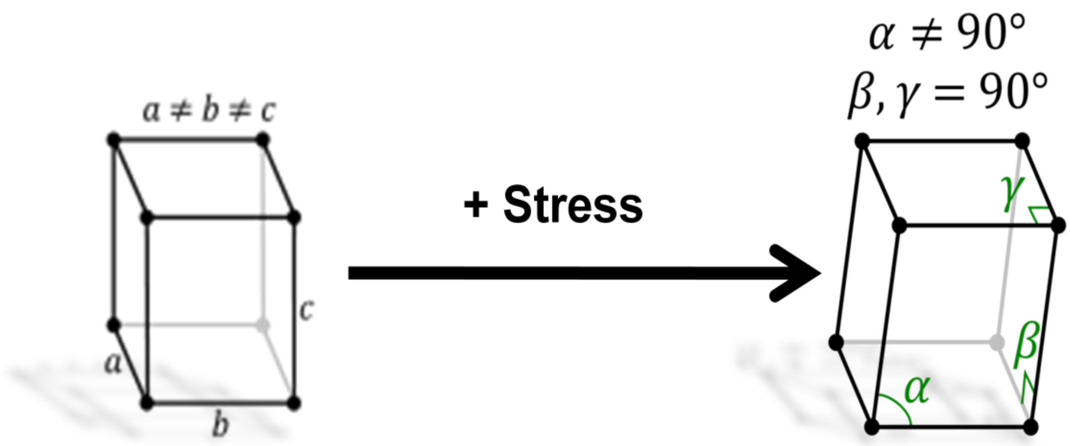

Figure 2.3: A schematic representing the stress-induced, tetragonal to monoclinic phase transformation in the in PSZ system.

In the presence of stress, a diffusionless phase transformation from tetragonal to monoclinic phase is induced (Figure 2.3), which in the case of YSZ, has an associated volumetric expansion of approximately 4%.[35] As a crack propagates, the exposed surfaces are allowed to transform. The surrounding matrix restricts volume expansion, which results in compressive forces on advancing crack tips and impedes further growth (Figure 2.4).

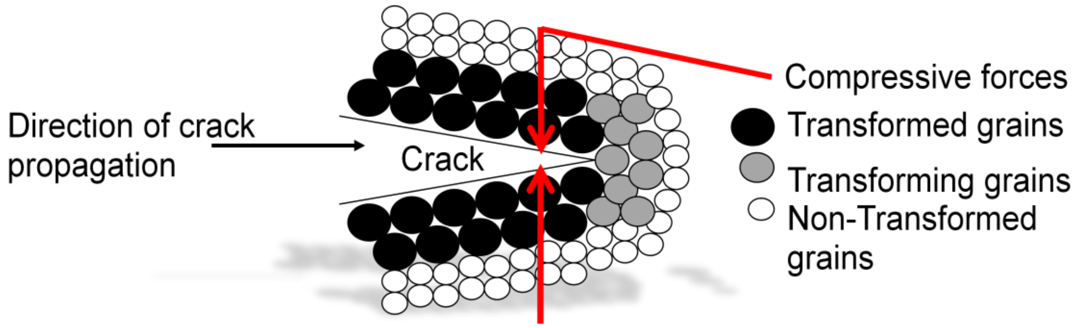

Figure 2.4: A schematic showing crack propagation trough a material employing the transformation toughening mechanism.

These forces can also induce a secondary micro-cracking toughening mechanism in the transformation zone, which generates a network of small, disordered cracks in the zone ahead of a propagating crack.[26] Generation of microcracks ahead of the crack front absorbs and distributes energy among multiple smaller cracks which would otherwise propagate a critical flaw.[26] This microcracking zone can also provide pathways for crack deflection of the advancing crack tip.

2.3 Dental Ceramics in Application & Fracture Behavior

The aforementioned toughening mechanisms can be experimentally observed through a technique called fractographic analysis or more simply, fractography. This technique utilizes analysis of a fracture surface for characteristic patterns.[27] By correlating features to crack velocities and directions, location of the fracture origin (critical flaw) can often times be determined. In practice, this technique yields insight into causes for failure. Furthermore, upon location of fracture origin, flaw size measurements allow for fracture mechanics principles to be applied to the system.

Many fracture mechanics principles rely on simplified geometrical representations of critical flaws. One such representation called the penny crack, or penny-shaped crack, represents a flat, circular or semi-circular crack in an infinite volumetric body.[42] Work by Lawn et al. utilized these techniques to effectively model the effect of point loads on the surface of a component.[43] This work significantly progressed fracture mechanics derivations associated with these types of flaw geometries. Later work further built on these techniques to evaluate and model residual surface stresses in brittle materials.[44]

2.4 Surface Modification of Dental Ceramics for Enhanced Mechanical Performance

Despite advancements in ceramic toughening methods, some applications inherently have competing goals that may unfavorably sacrifice fracture strength for alternative properties. For example, Fractography techniques applied to dental materials, led to the determination that clinically failed all-ceramic restoration failures were initiated at the surface, where tensile stresses and flaws were found to accelerate construct failure.[12, 45-49] In this system, clinical preparation methods of dental restorations employ roughening techniques to increase surface area for resin bonding. However, increased surface roughness provides numerous large flaw sites, increasing the likelihood of crack propagation and failure.[12-14] As a result, specimen fracture strength is exchanged for adhesion properties. Therefore, barring a complete overhaul of systems or procedures, ideal solutions improve limiting properties while allowing for current procedures to continue relatively uninhibited.

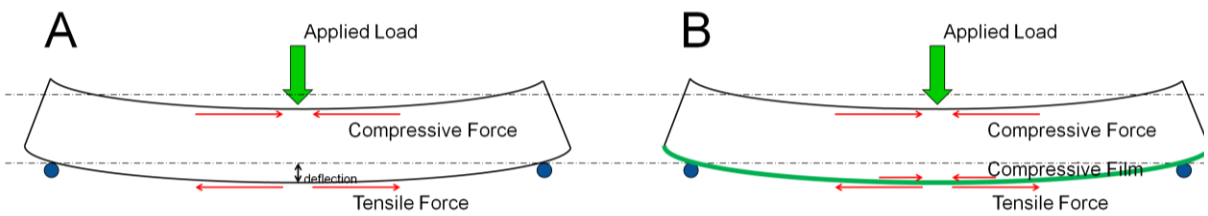

Figure 2.5: A Schematic showing A) The development of tensile and compressive forces on opposing sides of a component under 3-point flexure and B) The introduction of compressive surface forces opposes tensile forces under the same conditions.

One such class of solutions originates from inducing compressive surface stresses to a component in flexure. An idealized representation of flexural loading can be used to test flexural strength in a method known as 3-point bending or 3-point flexure (figure 2.5A). In flexural loading conditions, an applied load deflects a suspended beam specimen until fracture occurs. Due to an assumption of conserved volume, this loading profile generates maximum compressive stresses near the surface of an applied load and maximum tensile stresses on the opposing surface.[26]

As previously mentioned, toughening methods may be used to impart compressive residual surface stresses to counteract tensile forces and result in increased specimen strength. Applied to dental materials failure thermal treatments have been studied as a method to induce compressive surface stresses.[50-51] By utilizing differences in thermal expansion coefficients these treatments can be applied to dental coatings and glazes so that upon curing, they exist in a compressive state.[50-51]

However, for bilayer constructs, roughening techniques are used to promote adhesion and will relieve surface stresses. As a result, surface microcracking causes relaxation of inherent residual stress as well as increased tendency for failure, therefore causing this technique to be less practical in application. Techniques that allow for compressive stresses post roughening may be more suitable for dental applications. For example, ion implantation[52] and thin film coating techniques have been shown to improve ceramic flexural strength.[20, 22] Both techniques employ the excitation

2.5 Sputter Deposition

Thin film coatings allow for alteration of surface properties with minimal impact to physical component design or consumption of materials. One class of thin film deposition techniques, called physical vapor deposition (PVD), harness an energetic ejection of atoms from a target material towards a substrate. In sputter deposition, electrodes or ion beams are used to accelerate ions into a target material where upon collision with a target, momentum transfer causes ejection of target atoms towards a substrate.[53] Target atoms then coalesce into a film, with resulting film properties dependant on deposition parameters. Sputtering can be contrasted to evaporation processes, where thermal energy is the primary method for ejecting target atoms. However, sputter deposition allows for materials with high melting points or more complex stoichiometries to be grown.

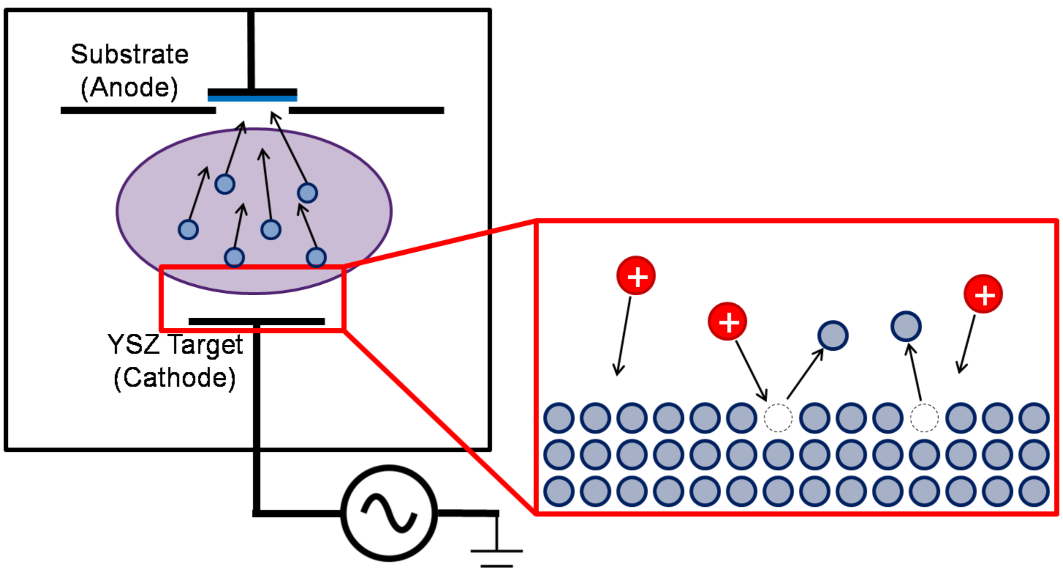

Figure 2.6: A schematic representing a typical sputtering chamber and the associated mechanism for ejection of target atoms.

A typical sputtering system consists of an evacuated chamber, containing parallel electrodes with opposing polarities (Figure 2.5).[53] A sputtering gas, typically comprised of a noble gas, is used to strike a plasma between the electrodes. The plasma ionization process can be described by the process below:

$$e^- + A \rightarrow 2e^- + A^+ \qquad \text{Eq. [2.8]}$$

where under a sufficiently large DC voltage carries an electron (e^-) towards the anode by an applied electric field. The electron collides with a neutral gas atom, producing a positively-charged ion (A^+) and another electron. Nearly instantaneously, the resultant electrons continue the reaction until a stable plasma is formed. The plasma then provides a source of positively charged ions which bombard towards the target.

However, the mechanisms of DC sputtering are confined to conductive materials such as metals. In a DC field, insulating materials (i.e. ceramics) will eventually reach charge neutrality and extinguish the plasma. To compensate for this issue AC current is employed and a second power source is coupled to the system (Figure 2.7). By oscillating current in the radio frequency range, allow electrons to be mobile enough to cause ionizing collisions and ions are mobile enough to sufficiently discharge electrodes within one cycle. Due to the greater mobility of electrons relative to ionic species, an r.f. system will self-bias to a negative potential on the cathode. A typical sputter deposition will generally employ a large anode surface area relative to the target as well as including magnetrons to confine plasmas near the surface of a target. As a result, the setup is termed an r.f. magnetron sputter reactor.

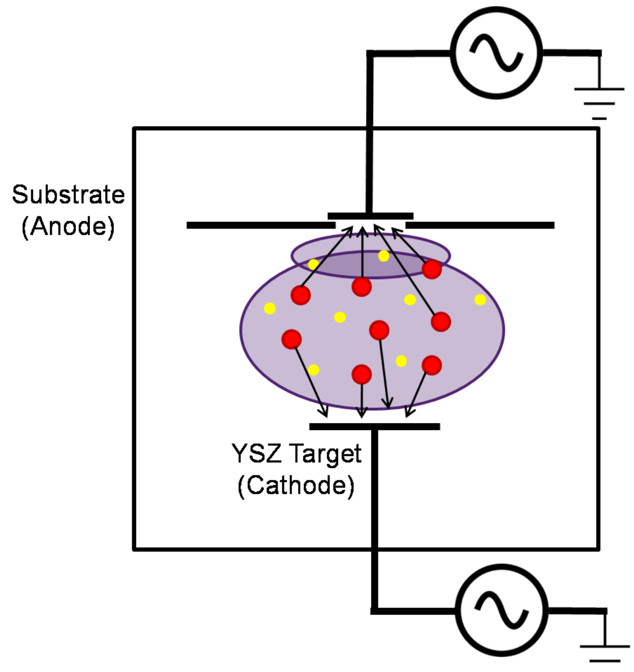

Figure 2.7: R.f. magnetron sputtering employs the use of a second AC power source attached to the anode of a sputtering system. The relative sizes of anode and cathode should be noted as an enhancing feature for r.f. sputtering. The additional power source also provides an additional processing variable, known as substrate biasing, to an r.f. sputtering system.

In r.f. sputtering, the additional power source can also provide an additional dimension of process variables known as substrate biasing (Figure 2.7). This parameter can induce acceleration of ionic species towards a substrate, similar to interactions at the target. As ions bombard a target or substrate surface, numerous interactions may occur including:

- Surface interactions:
  - Emission of target atoms (neutral), target ions, and/or secondary electrons,
  - Reflection adsorption of incident species
  - Diffusion of incident or target species
  - Generation of lattice defects due to displacement of atoms at the surface of the target or substrate.
- Bulk interactions:
  - Implantation of incident species
  - Densification or collapsing of voids in the target or substrate microstructure
  - Generation of lattice defects due to displacement of atoms within the target or substrate structure

2.6 Sputtering Parameters and Origins of Film Stress

The complex nature of sputtering and ionic interactions allow for a high degree of control over resulting thin film properties while also providing a nearly endless list of potential processing parameters. The key film properties in this work are residual stress and morphology. However other properties such as density, stoichiometry, deposition rate, optical and electrical properties can also be altered. Select parameters of interest to this work are discussed below:

As previously mentioned, substrate biasing induces ion bombardment at the substrate surface or surface of a growing film. During initial stages of film growth, ion bombardment can create charged sites on a substrate surface, resulting in improved film adhesion. During film growth, bombardment can increase film density, and consequently increase film hardness or residual stresses.

Deposition at elevated temperatures can provide enough thermal energy to allow impinging atoms to diffuse more readily than when in a reduced temperature state. As a result, larger, more equiaxed grains are typically grown at elevated temperatures. Additionally, when depositing at elevation temperatures, coefficient of thermal expansion (CTE) differences between film and substrate can induce large residual stresses at the interface. For example, when depositing a material with large CTE values relative to the substrate, cooling will cause an increased reduction in size for the film, relative to the substrate. Because the substrate is assumed to be much thicker than the film, the resultant system has the film in a tensile state relative to the substrate. Similarly, the opposite is true: Deposition of a material with a lower CTE than the substrate will result in a residually compressed film.

Working pressure is defined as the pressure at which a sputtering gas is injected into a chamber during deposition. For sputtering, these pressures generally range from ~1-25 mTorr.[53] This parameter can be visualized as the density of sputtering gas during deposition. As working pressure is increased, resultant collisions and interactions with the working gas reduce the mean free path of sputtered species. As a result ions generally bombard surfaces with a lower energy and angle of incidence relative to deposition at reduced working pressures.

Reactive gasses can also be injected during the deposition in a process known as reactive sputtering. In the ceramics, ejection of oxygen atoms from target surfaces can result in recombination of oxygen to molecular O_2, prior to reaching the intended substrate. Growing films will then have a stoichiometric deficit of oxygen relative to the target. To compensate, supplementary oxygen gas may be injected along with a standard inert sputtering gas.

During the sputtering process, kinetic energy of impinging atoms causes agglomeration of deposited atoms parallel to a substrate surface.[54-55] As film growth continues, proximity of atoms induces lattice expansion; however, expansion is inhibited by neighboring atomic clusters. As a result, compressive stresses along this plane are generated, while expansion in the direction perpendicular to the substrate remains uninhibited. This mechanism has been used to describe typical columnar film morphology in physical vapor deposited (PVD) films.[54-55]

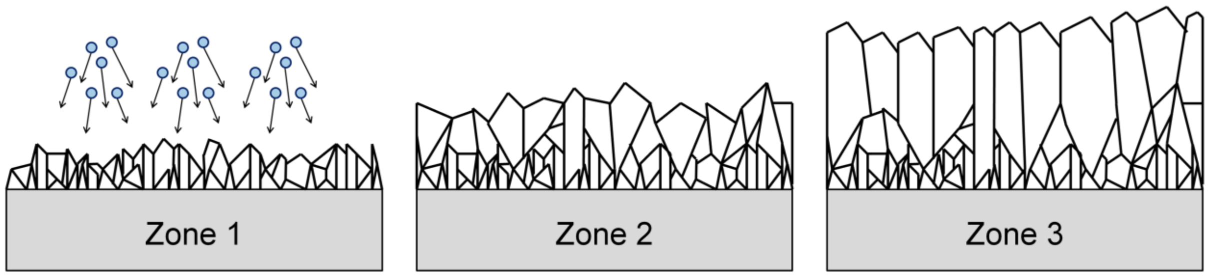

Figure 2.8: A schematic showing typical PVD film growth in through three distinct growth zones, resulting in a typical columnar microstructure [54].

PVD-deposited film microstructures typically display three distinct growth zones.[54-55] In this model, Zone 1 is described as the beginning of film growth, where randomly oriented grains nucleate and form grain boundaries upon coalescence. Zone 2 is a transitional zone where grains with preferred texture begin to overtake slower growing grains. Lastly, Zone 3 is characterized as steady-state grain growth, where the texture has fully evolved, and only the preferred growth direction remains, resulting in columnar microstructures. Film microstructures are also affected by temperature. As temperatures approach and exceed $T/T_m > 0.5$, recrystallization and grain growth mechanisms begin to dominate the resultant film morphology. Any changes in microstructure can be correlated to film properties (i.e. film stress), which are expected to vary between zones.

2.7 Deposition of Yttria Stabilized Zirconia Thin Films

Ruddell et al. has shown an alternative to thermal treatments by depositing a compressive metallic thin film on ceramic substrates via r.f. magnetron sputtering.[20]

Fracture strength testing of these specimens revealed improvements in fracture strength of up to 19% with less than 10μm of thin film. Another earlier work reported up to a 32% increase in fracture strength by using a multilayer film (10 μm) structure consisting of alternating layers of yttria-stabilized zirconia (YSZ) (1 μm) and parylene (1 μm).[23]

Studies by Amor et al. discussed correlations between select processing parameters (O_2 partial pressure, total pressure, r.f. power) and the resultant stoichiometries and optical properties of undoped, ZrO_2 thin films [Amor 1998]. Further work showed an ability to control sputtered, YSZ film stresses and morphology by varying parameters during deposition.[22, 57-59] Additionally, Teixeria et al. [21] reported a non-linear dependence of fracture strength on YSZ film thickness, with maximum fracture strength occurring at thicknesses of approximately 3 μm. Increases in strength were attributed to both crack bridging and blunting mechanisms. Crack bridging is due to the film spanning a crack tip, resulting in a reduction of crack-tip stress intensities.[21] In addition, compressive film stresses may enhance this effect by generating forces that oppose those required for crack propagation (under tensile loading) and counteracting the expansion of a crack. Furthermore, under certain deposition conditions, film growth may preferentially fill surface cracks and macroscopic defects leading to an increase in local radius of curvature, effectively blunting the sharp leading edge of a given flaw,[20] and increasing the external force threshold required for propagation.

This work aims to study the mechanical properties of PSZ-altered ceramic constructs as a viable method for improving the longevity and reliability of all-ceramic dental restorations. It has been proposed that the transformation-toughening and microcrack toughening benefits of bulk PSZ would translate to PSZ sputter-deposited thin-films. By applying a compressive, thin-film coating to all-ceramic substrates, is expected to provide strength advantages over current, clinical preparation methods.

CHAPTER 3: EXPERIMENTAL PROCEDURES

This chapter focuses on the methodologies used to prepare, modify, and characterize specimens. Sample preparation was centered on using a sputter deposition system to modify samples surfaces with 3mol% yttria-stabilized zirconia. It was observed that critical deposition parameters induced high compressive film stresses which resulted in significant improvements in fracture behavior of film-substrate constructs. Later studies quantified the effect of the film on specimens by depositing over an induced flaw. A flow chart of studies used in this work is outlined in figure 3.1 below, where sample preparation techniques and film deposition parameters were varied to quantify strengthening effects of compressive YSZ films on bulk mechanical properties. Analytical data was used to generate a predictive fracture stress model for compressive, thin-film modified substrates.

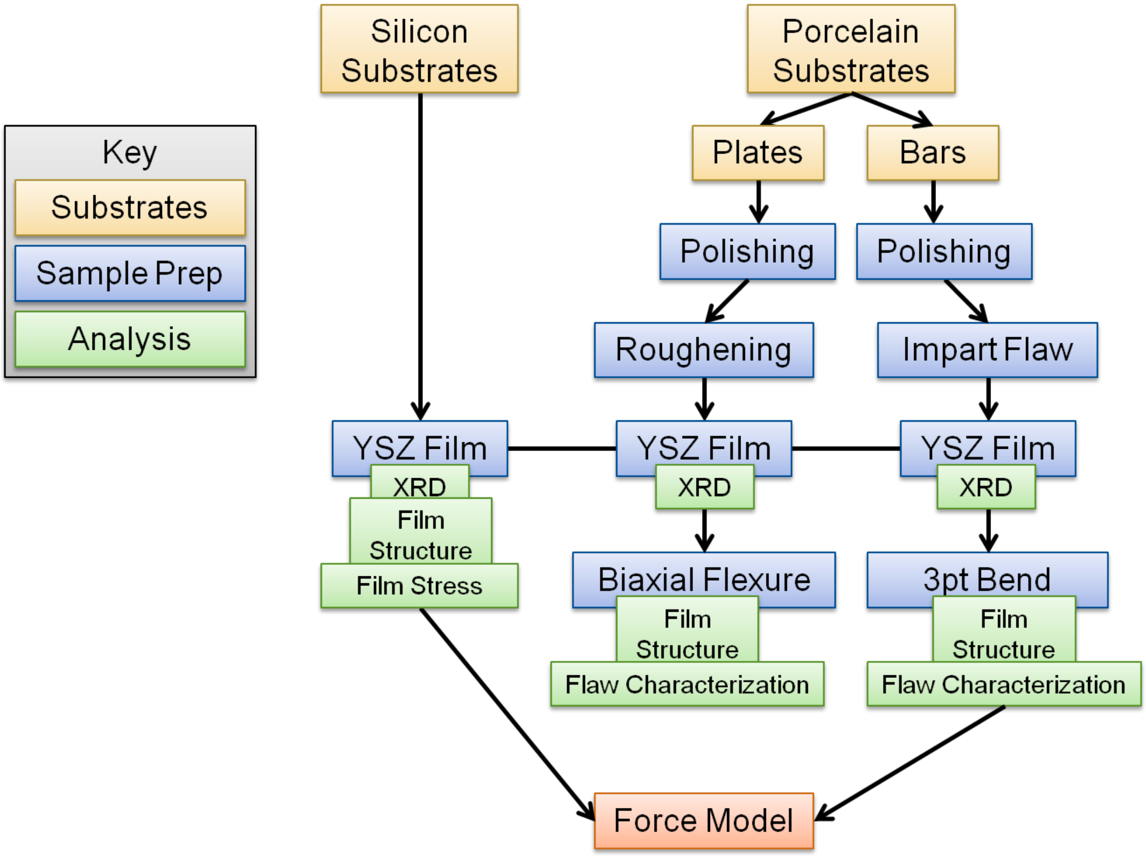

Figure 3.1: A flow chart outlining key methodologies and analytical techniques used in this work.

3.1 Substrate Materials and Preparation

Substrate materials used for initial film characterization were 4in diameter Silicon wafers (100 orientation). Substrates were manufacturer polished on one side and films were deposited on the roughened side to reduce likelihood of delamination. Subsequent experiments deposited films on diced silicon wafers (2x18mm) of varying thicknesses (0.5, 1, 2mm), glass wafers, and porcelain. Porcelain substrates were fabricated by cutting 12.5 x

12.5 x 1mm plates or 2 x 2 x 18mm bars from leucite-reinforced feldspathic porcelain blocks (ProCAD, Ivoclar-Vivadent, Schaan, Liechtenstein) having chemical composition of 6% Leucite in amorphous $KAlSi_2O_6$.

A standard preparation procedure was used for porcelain substrates that were subjected to fracture testing. Specimens were first mounted to a flat, stainless steel holder using adhesive wax so that multiple surface preparations could be conducted simultaneously. For each specimen, each surface was exposed to a polishing/grinding machine (Allied, Rancho Dominguez, California), at 250RPM. Surfaces were first polished using 250 grit sand paper until original surface features were removed. Polishing was continued until surface features were observed to be uniform on each specimen in an optical microscope. The process was repeated using 350, 400, 600, and 1200 grit sand paper until surface features were no longer observable in an optical microscope at 200x magnification. Samples were then unmounted then sonicated in an acetone bath to remove wax debris. Specimen edges were then rounded to prevent edge features and flaws from introducing error or voiding fracture studies.

Specimen surface preparation was continued through two methods, prior to film deposition. First, polished samples were subjected to air-abrasion with 50µm alumina for 10-15 seconds at a pressure of 0.28 MPa (40 psi) to simulate mechanical roughening in clinical use. These roughened surfaces were expected to provide greater surface area for film adherence, as delamination became evident on polished specimens. Second, as film adhesion methods were improved, specimen surfaces were normalized by using a Vickers indenter

(Mitutoyo Model AAV-500, Aurora, IL) to impart an indentation into the center of a polished substrate surface with indent corners perpendicular to substrate edges. Loads of 0.3, 0.5, and 1N were applied with a load time of 15 seconds, resulting in flaw sizes of 40, 70, and 100μm, respectively. Indent sizes and crack lengths were measured using an optical microscope (Sony DXC-390, Exwave HAD, Irvine, California) prior to and post film deposition to ensure flaw uniformity during fracture.

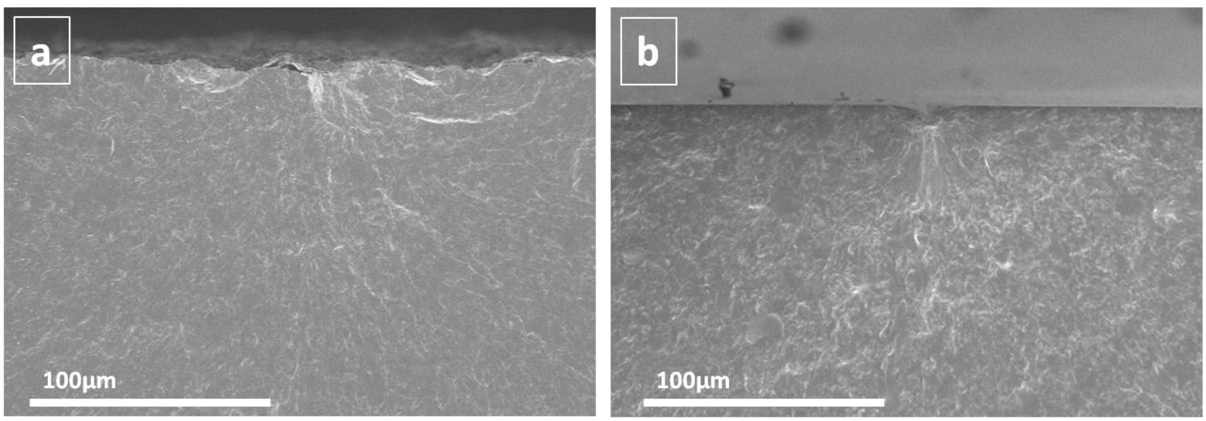

Figure 3.2: Image of a (a) critical flaw on a typical roughened surface as compared to (b) an indent used to simulate clinically-relevant critical flaws.

3.2 Deposition Parameters

Thin film coatings were performed via r.f. magnetron sputtering (CVC Model SC-400, Rochester, NY). Target material used for sputtering was 99.99% pure zirconia doped with 3mol% yttria (Plasmaterials, Livermore, CA). Substrates were mounted at a working distance of 75 mm, with the modified surface exposed to the target. For samples requiring substrate bias, a second r.f. power source was capacitively coupled to the substrate. Later methods incorporated a substrate pretreatment step to promote film adhesion. Here, a 50W substrate bias in 30:1 argon to oxygen atmosphere was applied for 5 minutes to clean organic debris from specimen surfaces prior to deposition. All depositions on fractured specimens were performed with a target power of 350 W, atmosphere of 30:1 argon to oxygen, and substrate bias varied between 0 and 100 W. Deposition rates were determined for each set of parameters and each substrate so that each specimen had the same film thickness. Specimens were then coated with 2-3μm of YSZ thin film to maximize fracture strength.[21]

3.3 Thin Film Characterization

Thin film properties were characterized primarily through non-destructive analytical techniques, including X-ray diffraction (XRD) (Rigaku SmartLab, The Woodlands, Texas) and Scanning Electron Microscopy (SEM) (Hitachi, S-4700 FE, Tokyo, Japan). XRD was used to characterize thin-film crystal structure by collecting diffracted x-ray intensity versus 2θ Bragg angle. XRD measurements were taken using a Cu Kα source at 40 kV and 30 mA over a 2θ range of 25° to 80° to capture the tetragonal and monoclinic peaks. An example of XRD plots for sputter-deposited, YSZ thin films are shown in figure 3.3. By removing background intensity (setting minimum points to zero intensity) and normalizing peak intensities to 100% of the most intense peak of each scan (Figure 3.3), data may be quantified and directly compared to each other.[59]

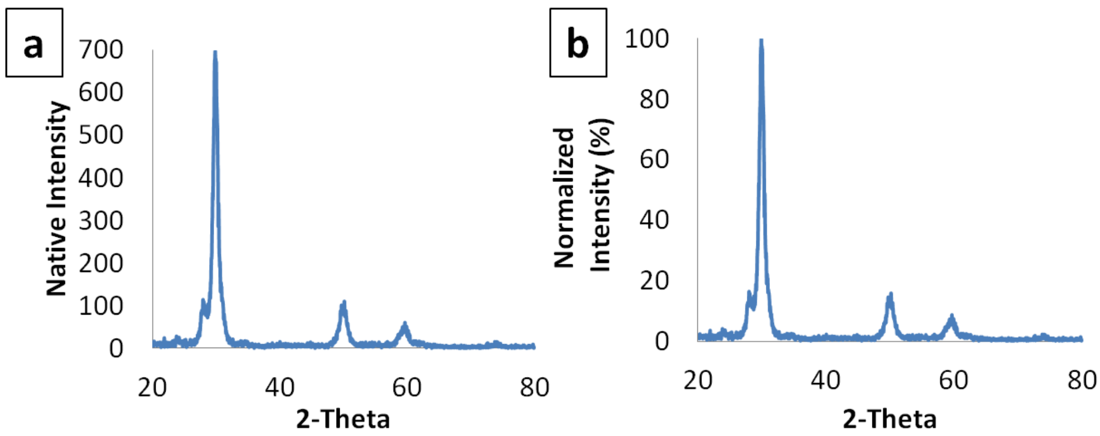

Figure 3.3: Example XRD data for a YSZ film deposited on a silicon wafer at 50W substrate bias showing (a) a native XRD plot showing intensity versus 2ϑ measurements, prior to normalization and (b) an example of the same XRD plot after normalization modifications.

Calculations are used to quantify the tetragonal and monoclinic phases within deposited films. A comparison of the relative intensities of the tetragonal ($I_{T(111)}$) and monoclinic ($I_{M(111)}$) peaks were used to determine volumetric percentage of monoclinic phase (V_M) as shown below (Eq. 3.1).[59]

$$V_M = \frac{2.379 * I_{M(111)}}{I_{T(111)} + 2.379 * I_{M(111)}} \qquad \text{Eq [3.1]}$$

Samples were then cleaved (if Si substrates) or fractured (if porcelain substrates) and fracture surfaces were evaluated using scanning electron microscopy (SEM) (Hitachi, S-4700 FE, Tokyo, Japan) and optical microscopy. Specimens were sputter-coated prior to analysis with gold-palladium to reduce charging effects in electron microscopy and to increase reflectivity in optical microscopy. Determination of failure modes was documented as well as cross-sectional film microstructure.

Wafer bow measurements (FLX-2300, Tencor, Milpitas, CA) were taken on the polished side of silicon wafers, prior to deposition, to measure film stress. Since measurements were taken on the opposite side of wafer in which films were deposited, measures tensile stresses were assumed to be compressive and vice versa. Post-deposition measurements were then taken, and radius of curvature values before and after deposition were compared according to the Stoney equation (Eq. 3.2) below.[60] In the Stoney equation for film stress, σ_f is the flexure strength, $E_s/(1-\upsilon_s)$ is the biaxial modulus of the substrate ($1.804*10^{11}$Pa), h is substrate thickness (525µm), t_f is film thicknesses, and R_o and R are initial and final radius of curvature measurements.

$$\sigma_f = \frac{-(E_s t_s^2)}{6(1-\nu_s)t_f}\left(\frac{1}{R}-\frac{1}{R_0}\right) \qquad \text{Eq. [3.2]}$$

These stress values were calculated based on assumptions about the film-substrate construct including: uniform film and substrate thickness, uniform stress across a surface, and equibiaxial curvature. Other assumptions are highlighted by Feng et al.[61] Although total film stresses can vary depending on substrate, intrinsic film stresses are independent of substrate. Therefore, trends in film stress in combination with XRD data were used to determine identical YSZ films on silicon and porcelain substrates.

3.4 Process Space Definition

Design of Experiments (DOE) software (DOE PRO XL, Sigma Zone, USA) was used to empirically calculate responses of interest over a range of input variables, while minimizing the need to run a full factorial of experiments. In this work, process variables of substrate bias and temperature were ranged from 0-100W and room-temperature 25°C-300°C, respectively on silicon substrates. Response variables included film stress, measured from wafer bow measurements and %monoclinic, measured from XRD. By measuring film stresses on silicon wafers, intrinsic film stresses can be calculated from equation 3.3 below

$$\sigma_F = \sigma_I + \sigma_T \qquad \text{Eq. [3.3]}$$

where σ_F is total film stress, σ_I is intrinsic stress, and σ_T is calculated thermal stress. Thermal stresses are calculated from equation 3.4 below

$$\sigma_T = E*\alpha*\Delta T \qquad \text{Eq. [3.4]}$$

where σ_T is thermal stress, E is young's modulus, α is thermal expansion coefficient, and ΔT is the change in temperature. Using these equations, film stresses can be calculated independent of substrates and for films deposited at varying deposition parameters. Process maps may be generated from these data as shown in figure 3.4 below.

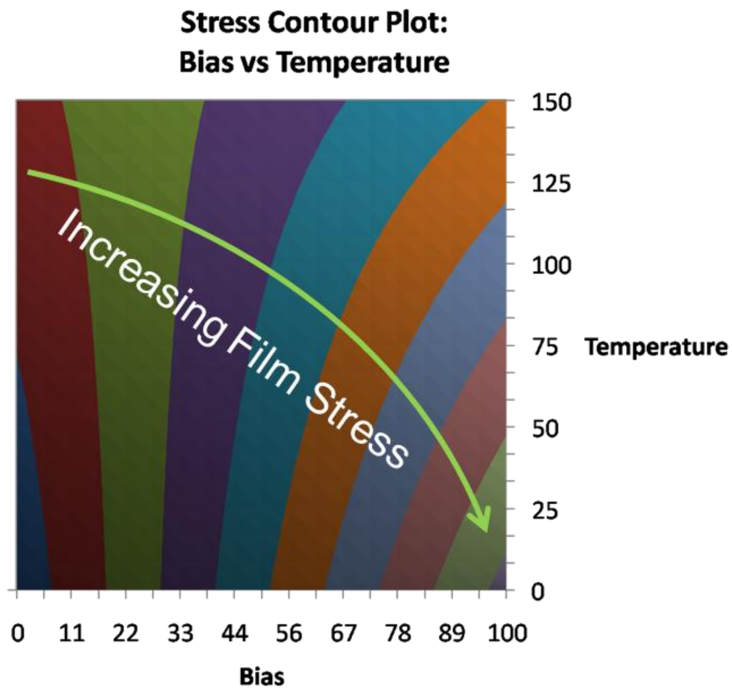

Figure 3.4: *A process map generated from DOE PRO XL software. Image shows compressive film stresses on Si for films deposited using varied substrate biases and temperatures.*

3.5 Fracture Characterization

Flexural strength was first determined by biaxial ring-on-ring testing in de-ionized water at 37ºC to simulate biological conditions.[21] Samples were then fractured in compression (Instron Model 5542, Norwood, MA) using custom fixtures, per ASTM Standard C1499.[62] Specimens were oriented with films in tension and loaded using a support ring diameter of 10mm and load ring diameter of 5 mm. Peak loads for each specimen were recorded then converted to fracture stress for each specimen using equation 3.5 below:

$$\sigma_e = \frac{3F(1-\nu)(D_S^2 - D_L^2)}{2\pi r^2 h^2 D^2}, D = 0.54(l_1 + l_2) \qquad \text{Eq. [3.5]}$$

Where σ is stress at fracture, F is peak load (N), v is Poisson's ratio (0.25), D_s is support ring diameter (10mm), D_L is load ring diameter (5mm), h is sample height (~1mm), and l is sample length (~12.5mm). For testing controls, two sample sets (polished and roughened) were unmodified by films in order to determine upper and lower bounds of substrate strengths, respectively.

Fracture strength was later determined on indented samples using a three-point bending fixture, with specimens oriented with films in tension per ASTM Standard C1161.[63] Testing conditions featured a 10 mm span and a crosshead speed of 0.5 mm/min in compression. Bar dimensions were measured prior to fracture for fracture stress calculations. Peak loads and fracture stresses for each specimen were recorded for sample sizes of n=30 and single-factor analysis of variance (ANOVA) at a 5% confidence level was performed to evaluate for statistical similarities. For testing controls, a polished sample set with a Vickers indentation was left unmodified by films in order to determine inert strengths of substrates at a given flaw size. Fracture strength and critical flaw size measurements then were used to calculate fracture toughness.[26] Flaw size and critical flaw location data were used to determine failure mode while Weibull analysis was used to analyze data from a mechanistic perspective.

3.6 Summary

Porcelain substrates were first modified using air abrasion with Al_2O_3 beads or by polishing and imparting a Vickers indentation in to the center of each specimen. Substrates were then exposed to a substrate bias to remove debris and to expose dangling bonds. 3mol% YSZ thin films were then deposited on to silicon and porcelain substrates. Thin-film-Silicon-substrate constructs were characterized by waferbow analysis, XRD, and SEM. Thin-film-porcelain substrates were characterized by fracture testing, XRD, and SEM. Fractography was conducted on fractured surfaces to determine critical flaw origin and mechanisms of failure. Fracture data was combined thin film stress calculations to develop a predictive fracture stress model for thin-film-substrate constructs.

CHAPTER 4: MICROSTRUCTURAL EFFECTS ON FRACTURE STRENGTH OF YTTRIA-STABILIZED ZIRCONIA (YSZ) THIN-FILM MODIFIED CONSTRUCTS

Submitted to the Journal of Biomedical Materials Research Part B: Applied Biomaterials

Running title: YSZ film microstructures for enhanced strength of bioceramics

Running Authors: Chan et al.

Ryan N. Chan

North Carolina State University, Department of Materials Science and Engineering, 911 Partner's Way, EB1 Room 3002, Raleigh North Carolina 27695 and RTI International, Center for Materials and Electronic Technologies, PO Box 12194, 3040 Cornwallis Rd. RTP, North Carolina 27709

Brian R. Stoner

RTI International, Center for Materials and Electronic Technologies, PO Box 12194, 3040 Cornwallis Rd. RTP, North Carolina 27709

Ronald O. Scattergood

North Carolina State University, Department of Materials Science and Engineering, 911 Partner's Way, EB1 Room 3002, Raleigh North Carolina 27695

Robert L. Smith

Nova Southeastern University, Section of Prosthodontics, 3301 College Avenue, Fort Lauderdale, Florida 33328

Jeffrey Y. Thompson

Nova Southeastern University, Section of Prosthodontics, 3301 College Avenue, Fort Lauderdale, Florida 33328

Jeffrey R. Piascik

RTI International, Center for Materials and Electronic Technologies, PO Box 12194, 3040 Cornwallis Rd. RTP, North Carolina 27709 and North Carolina State University, Department of Materials Science and Engineering, 911 Partner's Way, EB1 Room 3002, Raleigh North Carolina 27695

4.1 Abstract:

Recent investigations have shown an improvement in fracture strength in dental ceramics through sputter deposition of yttria-stabilized zirconia (YSZ) thin-films. It is hypothesized that films with differing microstructure and compressive film stress will further enhance a construct's fracture strength. YSZ thin-films were radio frequency (r.f.) sputter deposited with and without substrate bias (0-30W) on silicon and porcelain substrates. Wafer bow measurements were used to evaluate film stress magnitude, allowing for calculation of increases in compressive film forces (186N to 1688N with a thickness increase from 0.5μm to 8μm). Ring-on-ring flexure testing was performed on porcelain YSZ modified specimens and revealed an increase of 18% compared to an unmodified construct. Simple fractography allowed for critical flaw identification (average size 80μm) along with qualitative analysis of failure fracture energy while scanning electron microscopy (SEM) showed variations in film microstructure. Here, we propose a strengthening model that incorporates the effect of compressive thin-film forces on a critical surface flaw to further explain increased construct fracture strength.

4.2 Introduction

The corrosion and wear properties of ceramics, such as partially-stabilized zirconia (PSZ), along with the unique microstructures achievable by thin-film deposition, have made ceramic thin-films particularly appealing for use as protective coatings.[65-67] Furthermore, it has been shown that the application of thin-films to a dental ceramic can result in increased flexural strength.[20-21, 23] These strengthening properties are of particular interest in dentistry where common preparation techniques involve surface roughening by abrasion or etching to increase the bonding surface area of a construct.[68-69] However, these roughening techniques may also impart surface flaws, resulting in premature failure of a restoration. Under tension, surface flaws may act as potential stress-concentration and crack-initiation sites, allowing cracks to propagate more easily, thereby limiting the strength of ceramics.[12, 26, 70-72] By depositing PSZ films of varying microstructures and film stresses, this study aims to show a further increase in mechanical properties in PSZ-altered constructs while also developing a better understanding of strengthening mechanisms for thin-film coated ceramics.

PSZ is an attractive material due to its high fracture toughness relative to other ceramic materials (6-10 $MPa \cdot m^{1/2}$); attributed to phase transformation and microcrack toughening mechanisms.[26, 35-39] Transformation toughening is particularly apparent in PSZ, where dopants such as CaO, MgO, Y_2O_3, and/or CeO_2 can be used to stabilize high-temperature phases (cubic or tetragonal) of zirconia at room temperature.[40] The material system used in this study was 3mol% yttria-stabilized zirconia (YSZ), which has been widely reported to exist as metastable tetragonal phase at room temperature.[73] In the presence of stress, a diffusionless phase transformation from tetragonal to monoclinic phase is induced, which has an associated volumetric expansion of approximately 4%. Volumetric expansion then applies compressive forces on advancing crack tips, counteracting their propagation and resulting in increased fracture strength of the material. These forces can also induce a secondary, micro-crack toughening mechanism in the transformation zone, which generates a network of small, disordered cracks in the zone ahead of a propagating crack. Generation of microcracks absorbs energy which would otherwise propagate a critical flaw.[26] It has been proposed that the transformation-toughening and microcrack toughening benefits of bulk PSZ would translate to PSZ thin-films, further strengthening a construct.

Prior work from Ruddell et al. used radio frequency (r.f.) magnetron sputtering to deposit yttria-stabilized zirconia (YSZ) thin-films on porcelain[20] and alumina[22]. Their work demonstrated that fracture strength improvements of up to ~19% could be achieved from coating dental ceramics and other materials with less than 10 μm of thin-film PSZ. Teixeria et al.[21] reported a non-linear dependence of fracture strength on film thickness, with maximum fracture strength occurring at thicknesses of approximately 3 μm. Increases in strength were attributed to both crack bridging and blunting mechanisms. Crack bridging is due to the film spanning a crack tip, resulting in a reduction of crack-tip stress intensities.[74] In addition, compressive film stresses may enhance this effect by generating forces that oppose those required for crack propagation (under tensile loading) and counteracting the expansion of a crack. Furthermore, under certain deposition conditions, film growth may preferentially fill surface cracks and macroscopic defects leading to an increase in local radius of curvature, effectively blunting the sharp leading edge of a given flaw, and increasing the external force threshold required for propagation.[20]

Typical sputter-deposited YSZ thin-films display a highly columnar grain structure (Figure 4.1a). Such microstructures provide low-energy pathways for crack propagation and are considered to be non-ideal towards enhancing fracture strength. Using wafer bow measurements, Piascik et al.[56] reported that these structures also exhibited an increase in compressive film stresses over time when exposed to ambient environments. Increased film stresses were attributed to absorption of water molecules from the atmosphere into the intercolumnar porosity of the films. In an effort to densify the films and prevent water absorption, films were deposited using a substrate bias. This resulted in a unique morphology, characterized by randomly-distributed lateral defects throughout the film thickness (Figure 4.1b). This study aims to evaluate a model in which film structure is correlated to film stress and the impact of these stresses on a critical flaw and the resulting fracture strength.

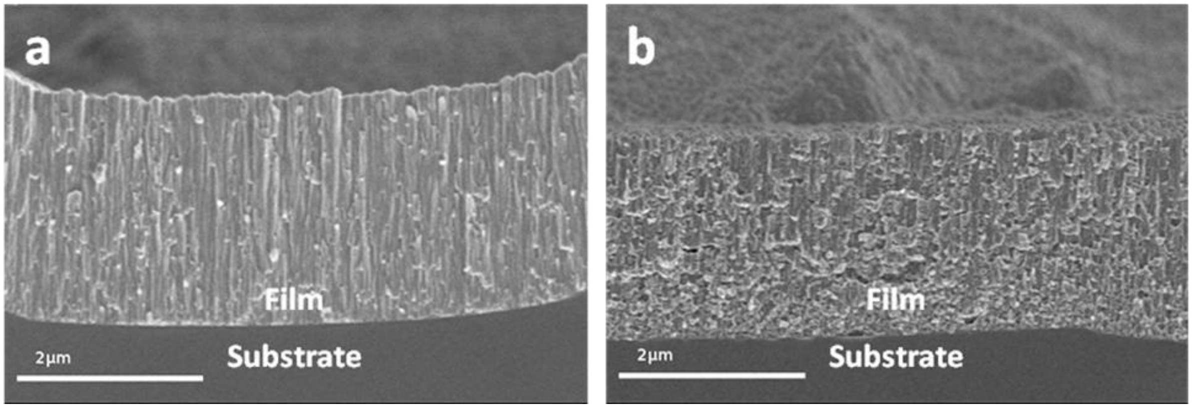

Figure 4.1: Representative SEM images of (a) film deposited without substrate bias and (b) film deposited with 20W substrate bias.

4.3 Experimental

YSZ thin-films were deposited on non-polished surfaces of single crystal silicon substrates (4inch diameter, (100), wafers) to simulate roughened surfaces of porcelain substrates (ProCAD, Ivoclar-Vivadent, Schaan, Liechtenstein). These roughened surfaces provide greater surface area for film adherence, as delamination was evident on polished specimens. Porcelain substrates were fabricated by cutting 12.5 x 12.5 x 1mm plates from leucite-reinforced feldspathic porcelain blocks (6% Leucite in amorphous $KAlSi_2O_6$). All porcelain substrates were polished through 1200 grit SiC abrasive and edges rounded to limit corner/edge failures. Polished surfaces of each specimen were then subjected to air-abrasion with 50µm alumina for 10-15 seconds at a pressure of 0.28 MPa (40 psi) to simulate mechanical roughening in clinical use. Substrates were ultrasonically cleaned in acetone to remove surface debris and randomly divided groups (n = 12).

Thin-film depositions were performed in an r.f. magnetron sputter reactor (CVC Model SC-400, Rochester, NY). A second r.f. power source was capacitively coupled to the substrate and used for depositions requiring a substrate bias. Target material used for sputtering was 99.99% pure zirconia doped with 3mol% yttria (Plasmaterials, Livermore, CA). Substrates were mounted directly above the sputtering gun (US Gun, San Jose, CA) in a custom fixture at a working distance of 75 mm. Once specimens were inserted into the chamber, the system was evacuated by a mechanical roughing pump, then by a cryogenic vacuum pump to a base pressure below $7x10^{-6}$ Torr. Sputtering gasses (30:1 Ar/O_2 gas ratio) were then introduced into the chamber and a plasma was ignited. All depositions were performed with a target power of 350 W and substrate bias was varied between 0 and 30 W. Based on prior work on the relationship between film thickness and flexural strength, films on porcelain substrates were grown to thicknesses of ~3 µm. Films on silicon were varied between 0.5 µm and 10 µm.

Films were characterized via X-ray diffraction (XRD) (Rigaku SmartLab, The Woodlands, Texas) to quantify the tetragonal to monoclinic phases within deposited films. A comparison of the relative intensities of the tetragonal ($I_{T(111)}$) and monoclinic ($I_{M(111)}$) peaks were used to determine volumetric percentage of monoclinic phase (V_M) as shown below (Eq. 1).[59]

$$V_M = \frac{2.379 * I_{M(111)}}{I_{T(111)} + 2.379 * I_{M(111)}} \qquad \text{Eq. (4.1)}$$

XRD measurements were taken using a Cu Kα source at 40 kV and 30 mA over a 2θ range of 25° to 80° to capture the tetragonal and monoclinic peaks. Samples were then cleaved (if Si substrates) or fractured (if porcelain substrates) and fracture surfaces were evaluated using scanning electron microscopy (SEM) (Hitachi, S-4700 FE, Tokyo, Japan) and optical microscopy for film microstructure and determination of failure modes. Specimens were sputter-coated prior to analysis with gold-palladium to reduce charging effects in electron microscopy and to increase reflectivity in optical microscopy. Wafer bow measurements (FLX-2300, Tencor, Milpitas, CA) were taken on silicon wafers prior to deposition. Post-deposition measurements were then taken, and radius of curvature values before and after deposition were compared according to the Stoney equation (Eq. 2) below[60]; where σ_f is the flexure strength, $E_s/(1-\upsilon_s)$ is the biaxial modulus of the substrate ($1.804*10^{11}$Pa), h is substrate thickness (525µm), t_f is film thicknesses, and R_o and R are initial and final radius of curvature measurements.

$$\sigma_f = \frac{-\left(E_s t_s^2\right)}{6(1-\nu_s)t_f}\left(\frac{1}{R} - \frac{1}{R_0}\right) \qquad \text{Eq. (4.2)}$$

These stress values were calculated based on assumptions about the film-substrate construct including: uniform film and substrate thickness, uniform stress across a surface, and equibiaxial curvature. Other assumptions are highlighted by Feng et al.[61] Although total film stresses can vary depending on substrate, intrinsic film stresses are independent of substrate. Therefore, trends in film stress in combination with XRD data were used to determine identical YSZ films on silicon and porcelain substrates.

Flexural strength was determined by biaxial ring-on-ring testing in de-ionized water at 37ºC to simulate biological conditions.[21] Samples were fractured (Instron Model 5542, Norwood, MA) using custom fixtures, per ASTM Standard C1499.[62] Specimens were oriented with films in tension and loaded using a support ring diameter of 10mm and load ring diameter of 5 mm. Peak loads for each specimen were recorded then converted to fracture stress for each specimen using equation 3

$$\sigma_e = \frac{3F(1-\nu)(D_S^2 - D_L^2)}{2\pi r^2 h^2 D^2}, D = 0.54(l_1 + l_2) \qquad \text{Eq. (4.3)}$$

Where σ is stress at fracture, F is peak load (N), v is Poisson's ratio (0.25), D_s is support ring diameter (10mm), D_L is load ring diameter (5mm), h is sample height (~1mm), and l is sample length (~12.5mm). For testing controls, two sample sets (polished and roughened) were unmodified by films in order to determine upper and lower bounds of substrate strengths, respectively.

4.4 Results and Discussion

YSZ films were first characterized by analyzing relative intensities of tetragonal and monoclinic peaks using XRD. Figure 4.2 reveals that for a deposited thin-film without substrate bias has ~19% monoclinic phase and increases to 87% when applying a 30 W substrate bias during deposition. This transformation is a result of a low-energy ion bombardment effect from the application of substrate bias during film growth. Upon bombardment, compressive film stresses are increased, inducing a tetragonal to monoclinic phase transformation in YSZ films.[56] Increased films stresses are expected to provide strengthening effects to YSZ-substrate.

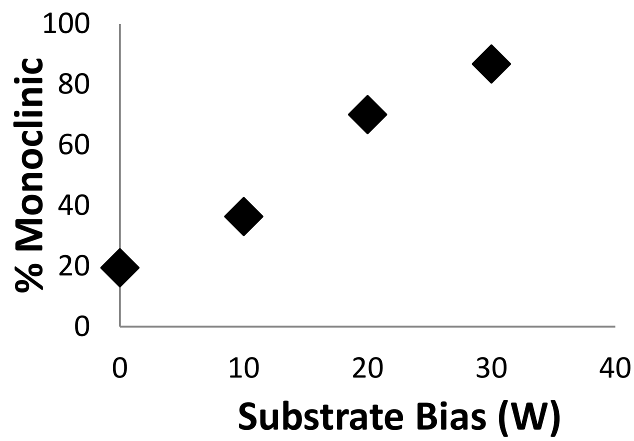

Figure 4.2: *An increase in %monoclinic phase from %19 - %87 can be observed with increasing substrate bias on porcelain substrates. As substrate bias is applied during film growth, a low-energy ion bombardment induces higher film stresses in YSZ, resulting in a tetragonal to monoclinic phase transformation.*

A material's strength is governed by its fracture toughness, where the values indicate a resistance to crack expansion and propagation. Fracture toughness values are determined by the size and shape of a sample's critical flaw. As shown in figure 4.3, optical micrographs of fractured porcelain specimens exhibit a semicircular shape with a radius of approximately 65µm.

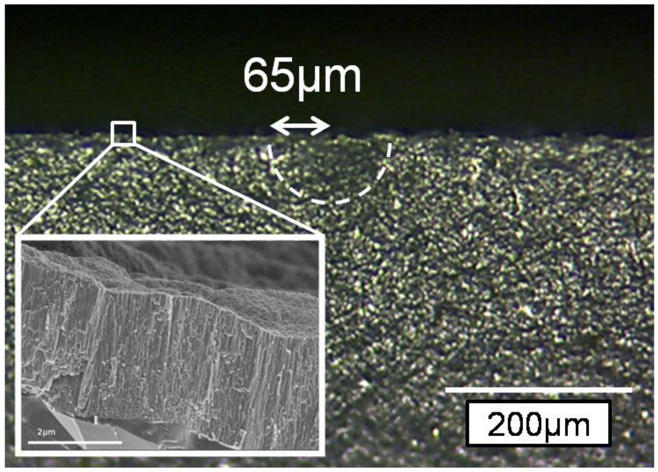

Figure 4.3: *An optical micrograph of a thin-film modified porcelain sample post fracture. Fracture surface, shows the size and semi-circular geometry of a critical surface flaw. Inset is an SEM micrograph, showing a YSZ film deposited without bias on the substrate surface.*

These semi-circular flaws can be modeled as a two-dimensional crack with a known cross sectional area. Under an applied load, tensile forces (F_A) will be applied over the area of a flaw which is opposed by a material's inherent strength (F_I) (Figure 4.4).

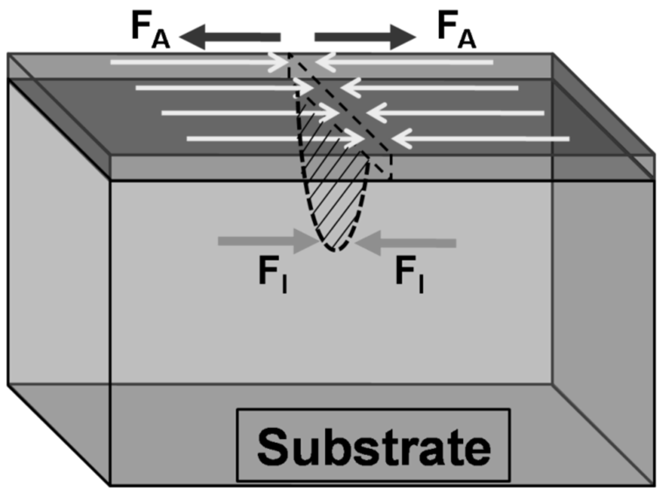

Figure 4.4: A model showing force vectors where compressive forces from YSZ thin-films are expected to act on a critical flaw, therefore increasing peak load at fracture and strengthening the construct. F_I indicates inherent compressive forces which oppose applied forces (F_A) until fracture.

When cumulative tensile forces exceed cumulative compressive forces, crack propagation occurs, resulting in failure. By depositing compressive thin-films on the surface, crack propagation will require additional tensile forces to overcome the combined compressive forces of the applied film and the inherent strength of the material, resulting in increased fracture strength.

By measuring film stresses as a function of thickness, the contribution of compressive film forces can be calculated from the equation:

$$\sigma = F/A \qquad \text{Eq. (4.4)}$$

where σ is film stress [MPa], F is force [N], and A is cross sectional area of the film [μm^2]. In this model, intrinsic film stresses are assumed to be uniform across the film thickness and independent of substrate, however effects of varying microstructure on stress will be discussed below. By assuming that all specimens are of the same width, magnitude of film forces can be normalized and qualitatively determined by multiplying film stress by film thickness. As shown in figure 4.5, compressive force on a critical flaw is expected to linearly increase from 186N to 1688N as film thickness increases from 0.5μm to 8μm.

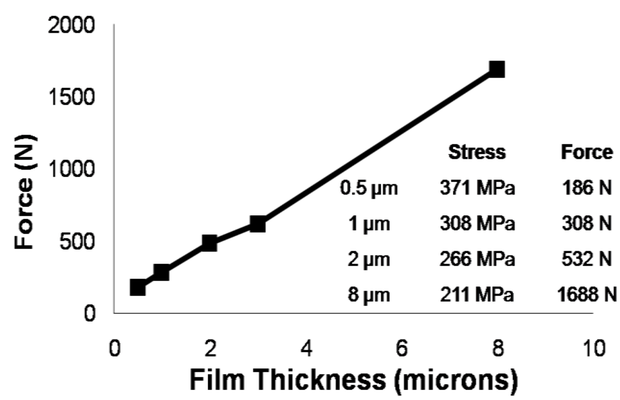

Figure 4.5: Film forces calculated as a function of film thickness showing an increasing force contribution.

As noted above, increases in compressive forces on a critical flaw are expected to result in fracture strength increases. However, as reported by Teixeira et al., thick films exhibit delamination due to interface failure from excessive film stresses, limiting the effectiveness of this film strengthening mechanisms.[21]

The proposed strengthening model (figure 4.4) assumes a uniform microstructure throughout the entire film thickness, whereas typical, PVD-deposited film microstructures typically display three distinct growth zones (figure 4.6).[55, 75-77]

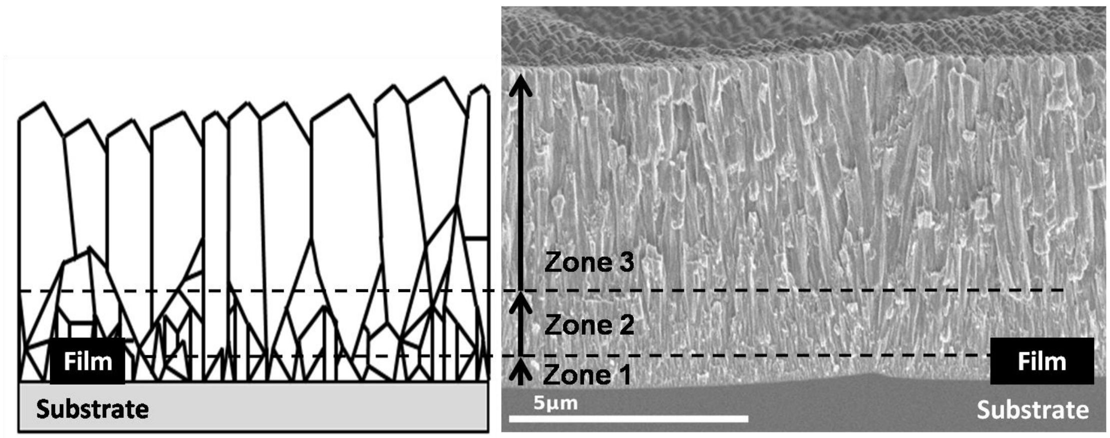

Figure 4.6: SEM micrograph of a typical deposited YSZ thin-film shows three microstructural growth zones resulting in columnar microstructures.

In this model, Zone 1 is described as the beginning of film growth, where randomly oriented grains nucleate and form grain boundaries upon coalescence. Zone 2 is a transitional zone where grains with preferred texture begin to overtake slower growing grains. Lastly, Zone 3 is characterized as steady-state grain growth, where the texture has fully evolved, and only the preferred growth direction remains, resulting in columnar microstructures. Due to changes in microstructure, film properties (i.e. film stress) are expected to vary between zones.

Although thicker films are expected to exhibit increased compressive forces, inter-granular boundaries of columnar grains (zone 3) are thought to more easily absorb atmospheric water vapor[78] and therefore be non-ideal for strengthening due to potential low temperature degradation (LTD) and/or sub-critical crack propagation effects.[79] YSZ thin-films were deposited at varying thicknesses to represent each microstructural zone and to study microstructural effects of atmospheric water absorption. Stress behaviors were measured over a period of 80 days as samples were exposed to the ambient environment. Results revealed that all thin-films were compressive (Figure 4.7), with the 3μm (zone 3) thin-film displaying the largest percent increase in stress, indicating the largest absorption of water vapor.

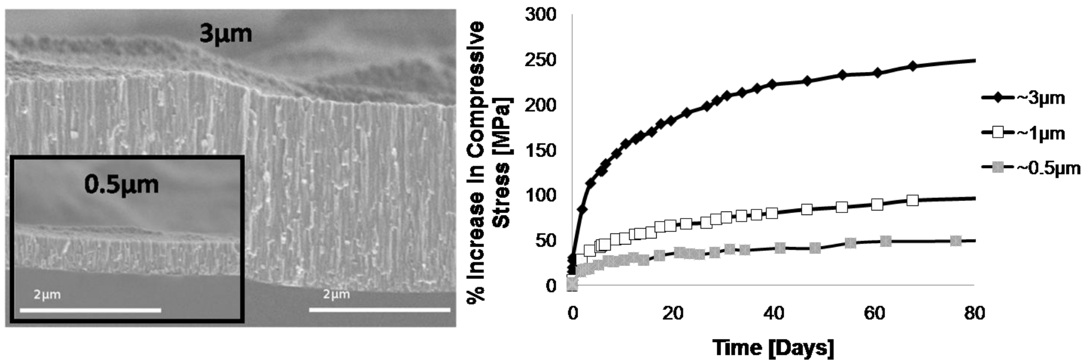

Figure 4.7: Stress behaviors of YSZ thin-films are correlated to microstructural development zones. By depositing identical films of varying thicknesses (without substrate bias), each zone can be represented, having a characteristic film stress response to atmospheric water absorption. This effect is exhibited by a % increase in film stress over a period of 80 days. SEM micrographs show the comparisons in morphology between a 3µm film and a 0.5µm (inset).

Alternatively, zone 1 films displayed the lowest percent increase in stress, indicating limited environmental effects. Data suggests stress behaviors can be used to characterize film microstructures and while zone 3 film thicknesses would provide optimum compressive forces for strengthening, zone 1 microstructures would provide optimum microstructural stability in a humid environment. Therefore an ability to produce thicker films (~3µm or greater) while maintaining control of film microstructure would result in the ability to optimize film stresses for enhanced strengthening effects.

YSZ microstructure alteration can be achieved through deposition with substrate bias [32]. As a result of increased ion momentum of impinging species on the growing film, a 3µm film deposited with a 20W substrate bias during deposition, results in an interrupted microstructure similar to a non-biassed, zone 1 film (Figure 4.1). Figure 4.8 shows similar stress behaviors of a 3µm film deposited with a 20W substrate bias, compared to a 0.5µm film deposited without substrate bias.

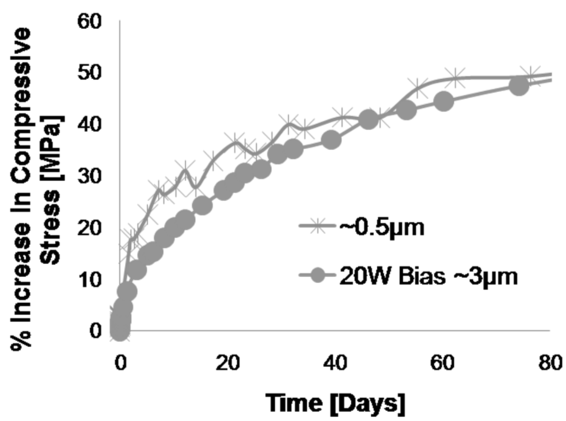

Figure 4.8: Percent change in compressive stress for 0.5µm film compared to 3µm film using substrate bias.

Here, we show that the desired microstructures of non-biassed, 0.5µm films can be replicated at increased film thicknesses (3µm) by applying a substrate bias during deposition. As supported by XRD measurements, films deposited with a substrate bias are therefore expected to induce increased compressive forces on a substrate surface and thus induce strengthening while also exhibiting improved environmental stability.

Biaxial testing was used to provide a more realistic stress distribution and simultaneously reduce potential edge effects that may occur as an artifact of uniaxial (3pt bend) testing.[64] Polished specimens exhibited reduced flaw sizes and therefore represent ideal fracture strength. Samples were then roughened to simulate clinically relevant procedures. Optical micrographs showing the differences between polished and roughened surfaces can be seen in Figure 4.9. YSZ films were then deposited on roughened surfaces with varying substrate biases.

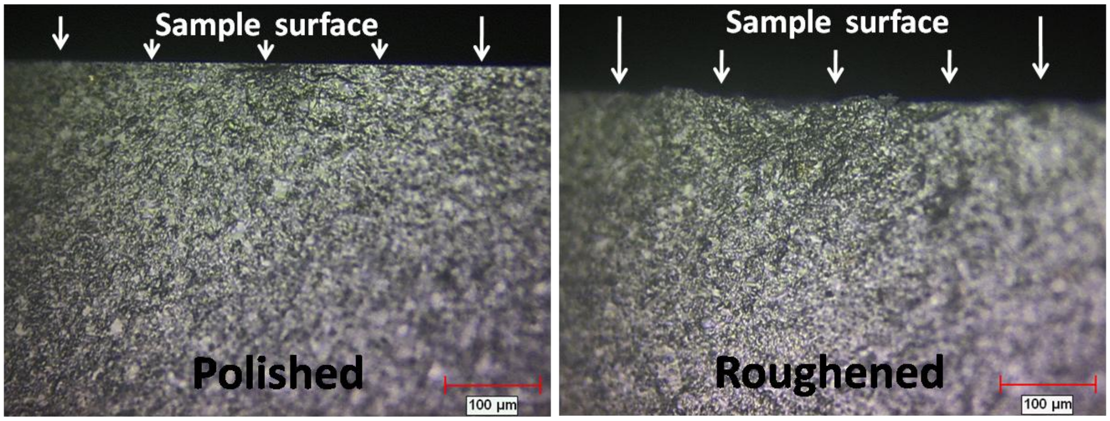

Figure 4.9: Representative optical micrographs of surface morphology of porcelain surfaces prior to and post air abrasion. R_a values for polished and roughened samples are 16nm and 990nm, respectively.

Biaxial data show an increasing trend in fracture strength from 0-20W substrate bias with a maximum improvement of ~18% (figure 4.10). Further improvement is expected with increasing substrate bias, however delamination was observed in higher biased samples (30W), resulting in lower fracture strengths relative to fully-adhered sample groups. Although ANOVA analysis shows roughened samples to be statistically similar, larger sample sizes and further experimentation with controlled flaw sizes are expected to show clearer trends in future experiments.

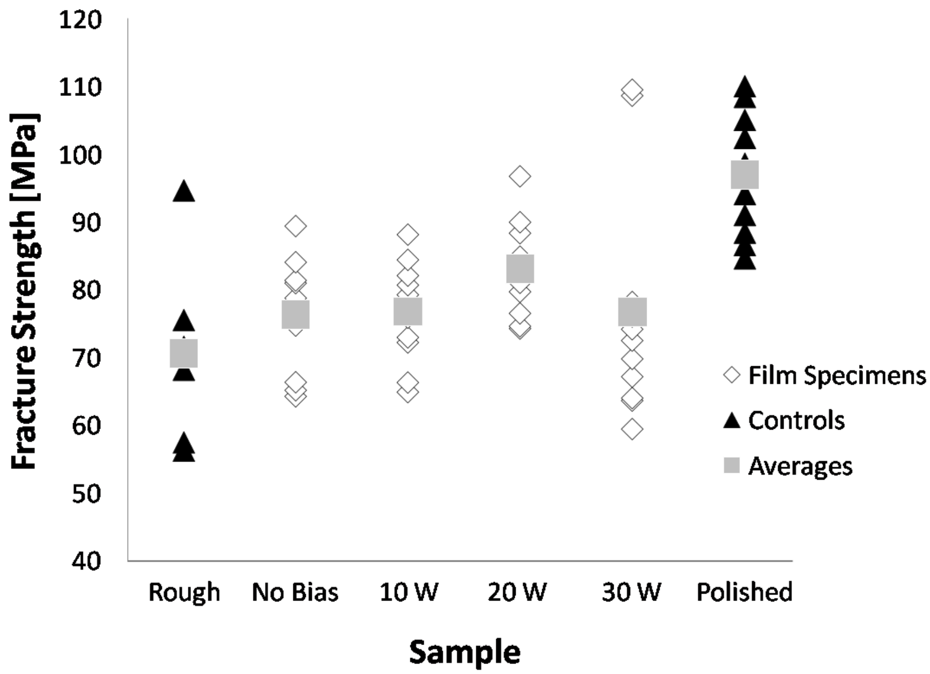

Figure 4.10: Biaxial fracture strength data for control samples and samples modified with 3µm thick YSZ films at varying substrate bias.

Fractography was used to qualitatively determine fracture energy of biaxial fracture specimens. This fracture energy arises from the conversion of elastic energy from flexure to the creation of new surfaces in the form of surface energy.[26] As seen in Figure 4.11A, increased fracture energy can be signified by the presence of increased secondary and tertiary cracking (increased surface energy)[60] and can be characterized as low, medium, and high fractures according to number of specimen pieces, post fracture.

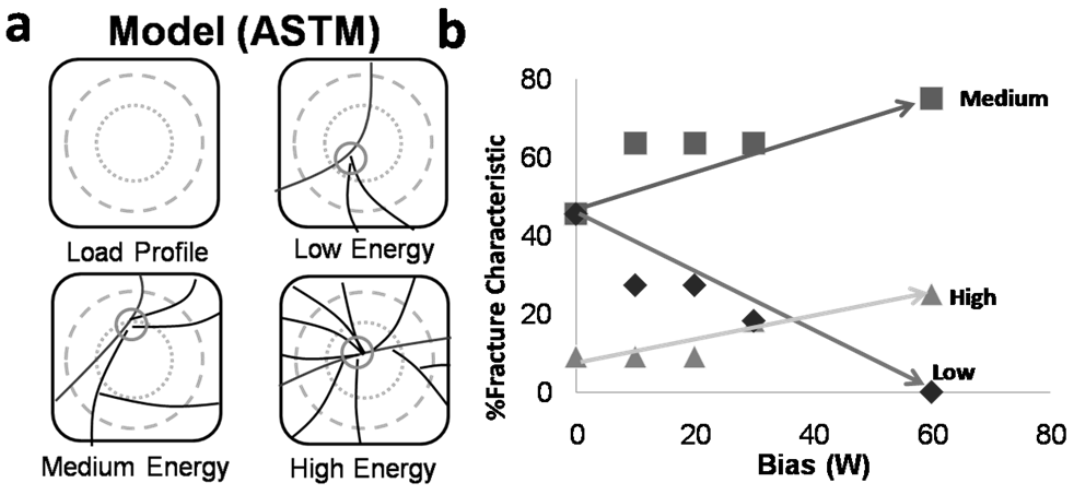

Figure 4.11: (a) Load profile and examples fracture patterns of biaxial fracture specimens and an optical image of a fractured specimen. (b) Characterized fracture behavior shows an increase in high and medium energy fracture characteristics at the expense of low energy fracture with increased substrate bias.

Results were compared among sample groups in Figure 4.9. Data show that with increasing substrate bias during deposition, an increase in medium and high energy fracture occurs at the expense of decreasing low energy fracture (figure 4.11B), indicating an overall increase in the energy required to fracture samples coated with the higher biased films. Fracture energy data support the hypothesis for biased, thin-film deposition as a viable method for ceramic substrate strengthening.

4.5 Summary and Conclusions

YSZ thin-films were deposited with varying microstructures on silicon wafers and dental porcelain by r.f. magnetron sputtering. While thicker films provide compressive forces on a critical flaw, columnar microstructures are thought to be non ideal due to their instability in aqueous environments. By applying a substrate bias during deposition, thicker films can be grown with zone 1, or disrupted microstructures. Control of these microstructures would therefore allow for film stresses and potentially other properties to be tailored to applications independent of film thickness.

Data from biaxial flexure suggest an increasing trend in fracture strength with increased substrate bias. This strengthening effect is attributed to resistance of crack expansion via forces in the film, which exert compressive forces on a substrate surface. A qualitative, fractography analysis of fractured specimens suggests an increasing trend in fracture energy versus substrate bias, supporting the ability to strengthen ceramic substrates with bias-assisted sputtered YSZ films. Further studies may work to reduce sample scatter and to further develop a structure-property model for the effect of compressive film stresses on the flexural strength of a ceramic construct.

Acknowledgements

This work is supported through NIH-NIDCR grant number NIH – 2RO1DE013511-10.

CHAPTER 5: FRACTURE TOUGHNESS IMPROVEMENTS OF DENTAL CERAMIC THROUGH USE OF YTTRIA-STABILIZED ZIRCONIA (YSZ) THIN-FILM COATINGS

Published in Dental Materials 2013:
R.N. Chan, B.R. Stoner, J.Y. Thompson, R.O. Scattergood, J.R. Piascik, (2013). Fracture toughness improvements of dental ceramic through use of yttria-stabilized zirconia (YSZ) thin-film coatings, Dental Materials, 29(8), 881.

Ryan N. Chan

North Carolina State University, Department of Materials Science and Engineering, 911 Partner's Way, EB1 Room 3002, Raleigh North Carolina 27695 and RTI International, Center for Materials and Electronic Technologies, PO Box 12194, 3040 Cornwallis Rd. RTP, North Carolina 27709

Brian R. Stoner

RTI International, Center for Materials and Electronic Technologies, PO Box 12194, 3040 Cornwallis Rd. RTP, North Carolina 27709

Ronald O. Scattergood

North Carolina State University, Department of Materials Science and Engineering, 911 Partner's Way, EB1 Room 3002, Raleigh North Carolina 27695

Jeffrey Y. Thompson

Nova Southeastern University, Section of Prosthodontics, 3301 College Avenue, Fort Lauderdale, Florida 33328

Jeffrey R. Piascik

RTI International, Center for Materials and Electronic Technologies, PO Box 12194, 3040 Cornwallis Rd. RTP, North Carolina 27709 and North Carolina State University, Department of Materials Science and Engineering, 911 Partner's Way, EB1 Room 3002, Raleigh North Carolina 27695

5.1 Abstract

Objectives: The aim of this study was to evaluate strengthening mechanisms of yttria-stabilized zirconia (YSZ) thin film coatings as a viable method for improving fracture toughness of all-ceramic dental restorations.

Methods: Bars (2x2x15mm, n=12) were cut from porcelain (ProCAD, Ivoclar-Vivadent) blocks and wet-polished through 1200-grit using SiC abrasive. A Vickers indenter was used to induce flaws with controlled size and geometry. Depositions were performed via radio frequency magnetron sputtering (5mT, 25ºC, 30:1 Ar/O_2 gas ratio) with varying powers of substrate bias. Film and flaw properties were characterized by optical microscopy, scanning electron microscopy (SEM), and x-ray diffraction (XRD). Flexural strength was determined by three-point bending. Fracture toughness values were calculated from flaw size and fracture strength.

Results: Data show improvements in fracture strength of up to 55% over unmodified specimens. XRD analysis shows that films deposited with higher substrate bias displayed a high %monoclinic volume fraction (19%) compared to non-biased deposited films (87%), and resulted in increased film stresses and modified YSZ microstructures. SEM analysis shows critical flaw sizes of 63$\pm$1µm leading to fracture toughness improvements of 55% over unmodified samples.

Significance: Data supports surface modification of dental ceramics with YSZ thin film coatings to improve fracture strength. Increase in construct strength was attributed to increase

in compressive film stresses and modified YSZ microstructures. It is believed that this surface modification may lead to significant improvements and overall reliability of all-ceramic dental restorations.

5.2 Introduction

All-ceramic dental restorations have become extremely popular due to their outstanding aesthetic characteristics and biocompatibility.[80-83] However, these materials, when placed in load bearing applications, often display an inability to resist stress-induced crack propagation.[26, 72, 84] Analysis of clinically failed all-ceramic restorations revealed that the majority of failures were initiated at the surface, where tensile stresses and flaws were found to accelerate construct failure.[12, 46-49, 81] Additionally, clinicians typically etch or particle air-abrade to roughen surfaces for enhanced adhesion, inducing large surface flaws and further promoting premature failure.[12-14, 60, 85] This study seeks to modify surface stress states and facilitate flaw modification to increase the fracture toughness of dental porcelain.

Fracture toughness improvements have been demonstrated through various surface modification methods; such as, flaw modification, heat treatments, and coatings. Fundamentally, by controlling surface finishing techniques, fracture toughness can be enhanced through modification of flaw size or geometry, resulting in reduced stress concentration in the local area of a critical flaw and therefore increasing overall strength of a sample.[12, 15] Compressive stress gradients can also be introduced to a sample through thermal processing, where a surface is cooled at a faster rate than the interior of a sample, resulting in a compressive surface.[17-18] Composition gradients and ion implantation techniques have also been used to induce strain into the crystal lattice, resulting in compressive stresses on a sample surface.[19] These stress-modification mechanisms require crack expansion (or increased tensile stresses), to overcome the induced compressive stresses on the surface of a sample. As a result, crack propagation is inhibited, resulting in increased fracture toughness.

Thin film coatings have been employed to strengthen substrates; first through critical flaw modification and secondly through inducing compressive surfaces stresses.[20-21] Ruddell et al. has shown improvements in fracture strength of up to 19% by coating ceramic substrates with less than 10μm of sputtered metallic thin films.[20, 22] Earlier work reported increases in strength of up to 32% by using a multilayer film (10 μm) structure consisting of alternating layers of yttria-stabilized zirconia (YSZ) (1 μm) and parylene (1 μm) to induce crack deflection.[23] Additionally, it was determined that a 2-3 μm thick YSZ thin film sputtered on porcelain substrates provide the maximum benefit for increased construct fracture strength.[21]

YSZ is a material of particular interest not only due to its biocompatibility, but also for its excellent wear resistance properties.[86-88] Reports have shown that microstructure and film stress properties of YSZ thin films can be tailored through the control of deposition parameters.[57, 89] By applying a substrate bias during deposition, an interrupted microstructure consisting of lateral microcracks and increased compressive films stresses can be obtained. It is therefore hypothesized that these structures may provide an ideal thin film for increasing the fracture toughness of ceramic substrates.

This study examines the benefits of varying YSZ thin film microstructures and magnitudes of compressive thin film states on substrates that have been fabricated with a controlled flaw size of a given geometry. Analysis of construct fracture strength and measurements of critical flaw size allows for the determination of overall construct fracture toughness. Here we discuss the impact of thin-film induced compressive stresses, flaw modification, and crack deflection on increased fracture toughness of modified dental porcelain.

5.3 Experimental

Porcelain substrates were fabricated by cutting 18 x 2 x 2 mm bars from leucite-reinforced feldspathic porcelain blocks (ProCAD, Ivoclar-Vivadent, Schaan, Liechtenstein). All four surfaces of porcelain substrates were polished through 1200 grit SiC abrasive and edges rounded to limit corner/edge failures. Substrates were ultrasonically cleaned in acetone to remove surface debris prior to deposition, then randomly divided into groups (n=30). A Vickers indenter (Mitutoyo Model AAV-500, Aurora, IL) was used to apply a single, controlled flaw into the substrate surface with indent corners perpendicular to substrate edges, in order to normalize failures through control of critical flaw size and geometry. A 0.5N load was applied with a load time of 15 seconds, resulting in an indent size of 35$\pm$2μm to simulate critical flaw sizes in clinical surface preparation methods.[46]

Thin-film depositions were performed in an r.f. magnetron sputter reactor (CVC Model SC-400, Rochester, NY). A second r.f. power source was capacitively coupled to the substrate and used for depositions requiring a substrate bias. Target material used for sputtering was 99.99% pure zirconia doped with 3mol% yttria (Plasmaterials, Livermore, CA). Substrates were mounted directly above the sputtering gun (US Gun, San Jose, CA) in a custom fixture at a working distance of 75 mm. At the start of each deposition, a 50W substrate bias in an argon atmosphere was applied for 5 minutes to clean organic debris from sample surfaces and to promote film adhesion. All depositions were performed with a target power of 350 W, atmosphere of 30:1 argon to oxygen, and substrate bias varied between 0 and 100 W. Films were grown to a thickness of 2-3μm to maximize fracture strength.[23]

X-ray diffraction (XRD) (PANalytical X'Pert PRO MRD HR, Westborough, MA) was used to determine the percentage of tetragonal and monoclinc phases[59] in the YSZ films and thus qualitatively determine trends in film stress.[56] Fracture strength values were determined using a three-point bending fixture, with specimens oriented with films in tension per ASTM Standard C1161.[63] Flexural testing (Instron Model 5542, Norwood, MA) was conducted with a 10 mm span at a crosshead speed of 0.5 mm/min. Peak loads and fracture stresses for each specimen were recorded and single-factor analysis of variance (ANOVA) at a 5% confidence level was performed to evaluate for statistical similarities. For testing controls, a polished sample set with a Vickers indentation was left unmodified by films in order to determine inert strengths of substrates at a given flaw size. Post fracture, scanning electron microscopy (SEM) (Hitachi, S-4700 FE, Tokyo, Japan) and optical microscopy (Sony DXC-390, Exwave HAD, Irvine, California) was used to image sample fracture surfaces to characterize critical flaws. Fracture strength and critical flaw size measurements then were used to calculate fracture toughness.[26]

5.4 Results

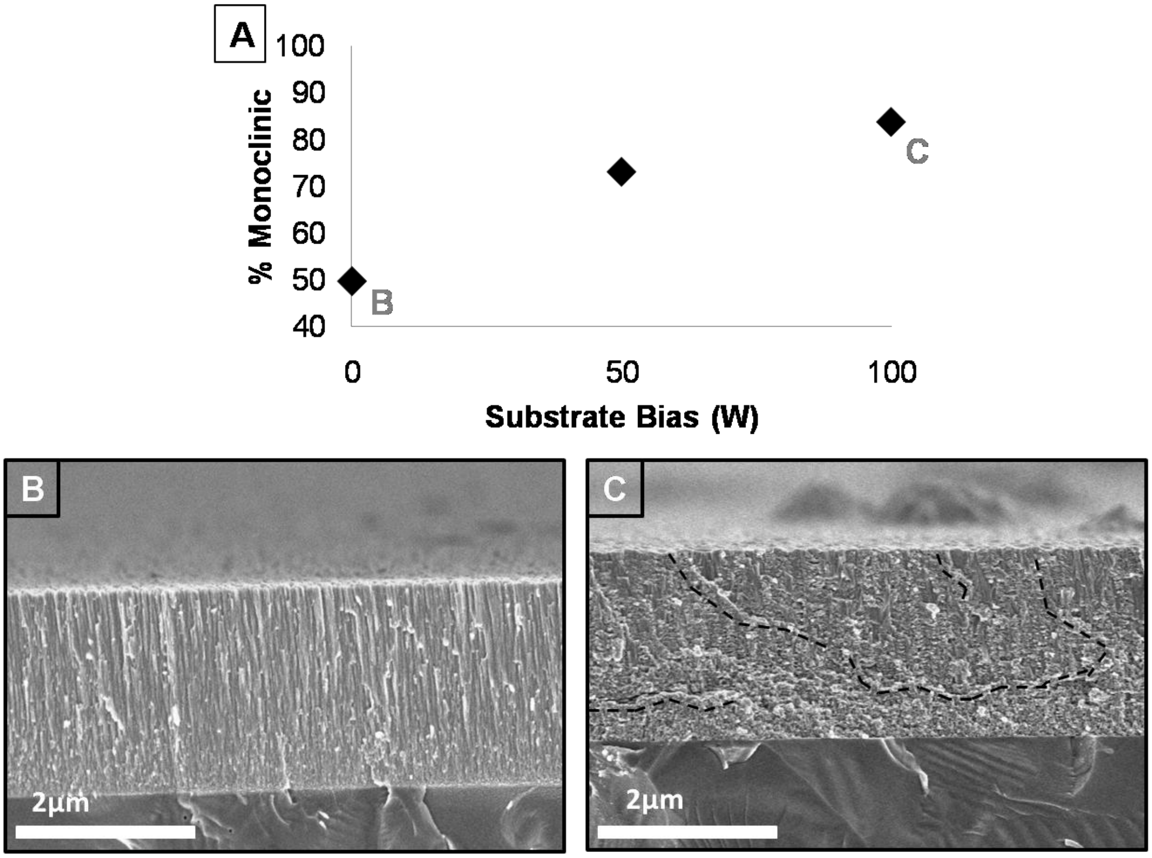

Figure 5.1: (a) X-ray diffraction data show an increase in %Monoclinic phase as a function of substrate bias, indicating an associated increase in compressive film stresses. SEM images of fracture surfaces showing microstructure differences between films deposited (b) without substrate bias (c) with 100W substrate bias. Changes in microstructure suggest a potential crack deflection strengthening mechanism, highlighted by dotted lines.

%Monoclinic vales were found to increase with substrate bias (Figure 1A), ranging from 50% (no substrate bias) to 84% (100W substrate bias). Observable changes in film microstructure were associated with increasing volume fraction of %monoclinic. A representative SEM image of a non-biased film structure (Figure 1B) was shown to have a columnar morphology; whereas, 100W film (Figure 1C) shows interrupted structure with characterized by the presence of inter-granular ledges.

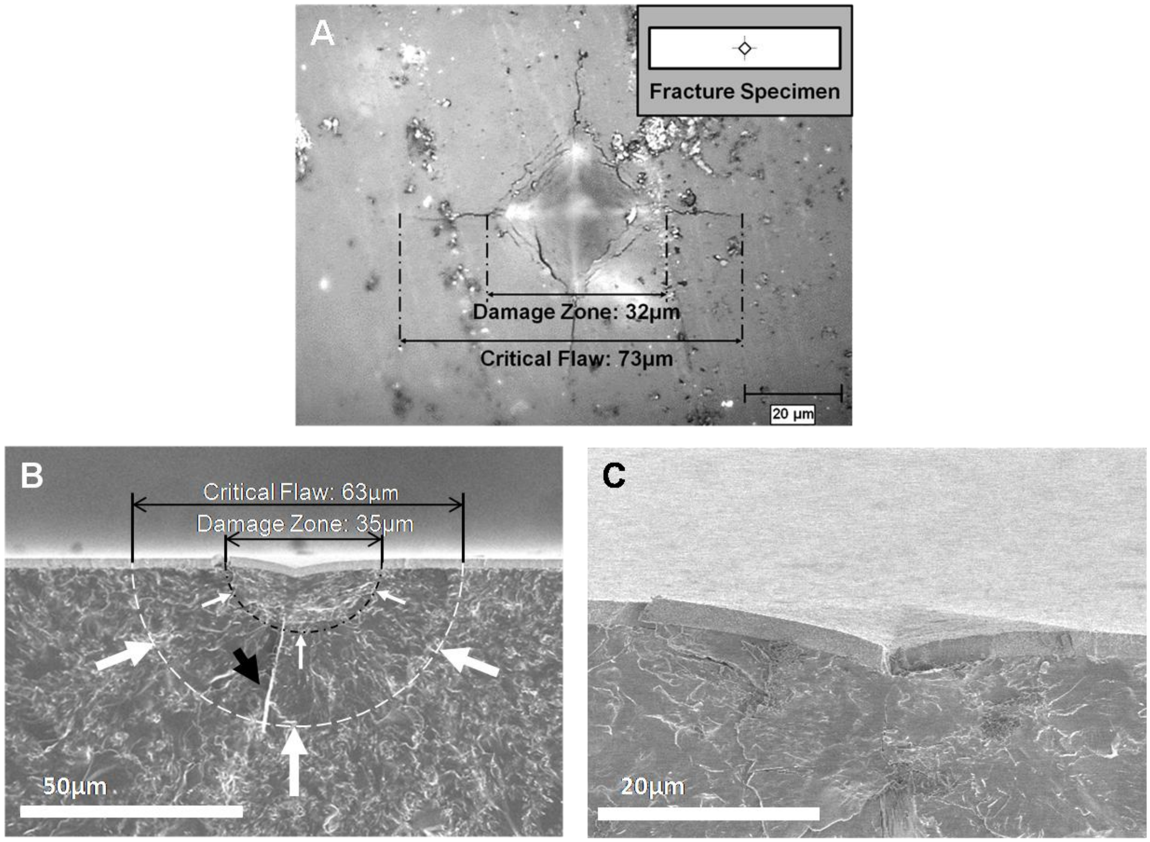

Figure 5.2: *(a) Optical micrograph showing a 35±2µm Vickers indent on the surface of a porcelain substrate. Radial cracks denote size of critical flaw. Inset shows flaw orientation on an example fracture specimen. (b) SEM micrograph of a fracture surface showing characteristics of a critical flaw as a result of Vickers* indentation. Critical flaw diameters are measured to be 63±1µm. (c) After sputter depositing a YSZ thin film, SEM micrograph demonstrates good adhesion to a Vickers indent and the substrate surface.

In order to standardize critical flaw size, a Vickers indent was applied to each surface prior to thin film deposition and characterized. Figure 2A is a representative optical image of an indent that shows the damage zone (35±2μm) and critical flaw size (63±1μm) characterized by the radial cracking from the indent corners. Figure 2(B) shows a critical flaw on the fracture surface of a fractured specimen. A damage zone can be seen in the area immediately under the indent (indicated by small arrows), from which the radial cracks identify the size of critical flaw (indicated by large arrows). Radial crack traces, perpendicular to the fracture surface (beyond the borders of the micrograph), can be observed (indicated by black arrow). Additionally, Figure 2(C) shows a post-fracture sample indicating failure at the indent (critical flaw) and excellent adhesion between the thin film and porcelain.

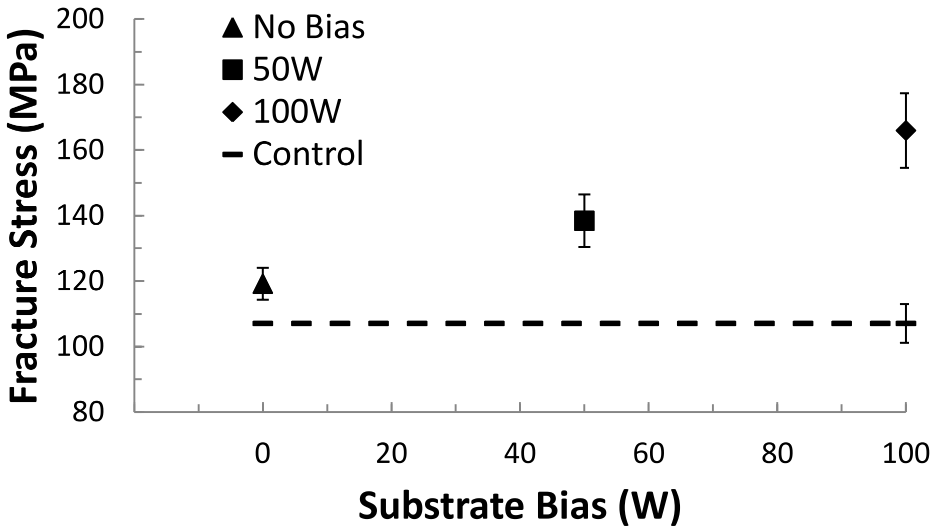

Figure 5.3: *Fracture stress values measured from 3pt bend flexure testing. The straight line indicates fracture strength for control samples. Data shows an improvement in fracture strength of 55% over unmodified substrates. Error bars represent 95% confidence levels.*

Figure 3 shows fracture strength values for control samples and samples modified by YSZ thin films. Unmodified specimens showed fracture strengths of 107±6 MPa. Samples coated with unbiased thin films displayed a fracture strength of 119±5 MPa; whereas, samples coated with thin films deposited at 100W substrate bias showed fracture strength of 166±11 MPa. Fracture stress increased over unmodified samples ranging from 14-55% and ANOVA analysis showed that all sample groups were statistically different

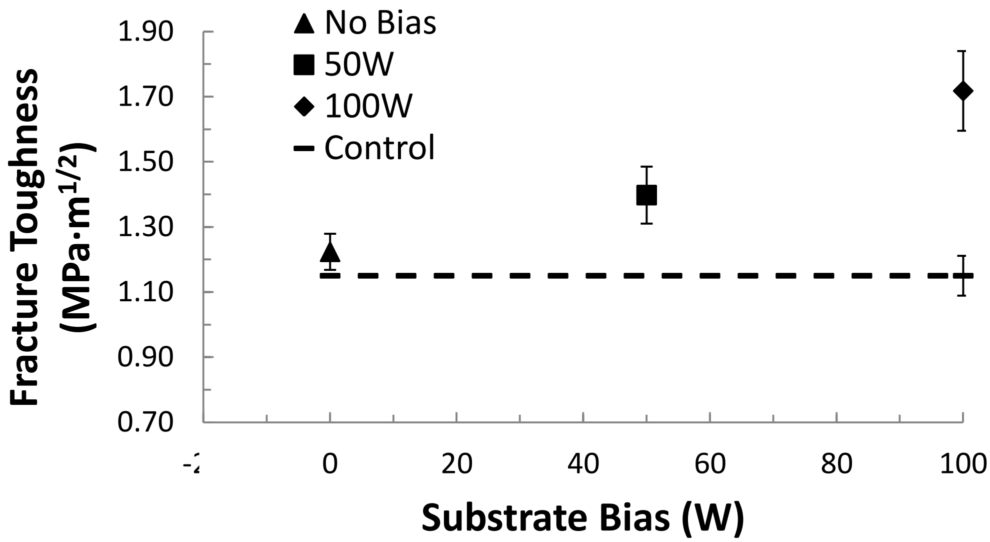

Figure 5.4: Fracture toughness values calculated from 3pt bend fracture strength data and flaw size measurements. By depositing a YSZ film with 100W substrate bias, an improvement in fracture toughness of 55% can be attained over unmodified substrates. Error bars represent 95% confidence levels.

Fracture strength and flaw size measurements were used to calculate fracture toughness values for each sample (Figure 4). Fracture toughness calculations used the equation

$$K_{IC} = Y\sigma_f\sqrt{a} \qquad [1]$$

where K_{IC} is the mode I critical stress intensity factor (fracture toughness) [MPa$\sqrt{\text{m}}$], Y is the shape factor (1.29), σ_f is fracture stress [MPa], and a is the radius of the critical flaw [m].[27]

Fracture toughness shows similar trends to fracture strength (increases of 14-55%). Literature values show porcelain fracture toughness at approximately 1.0 MPa·m$^{1/2}$ [27, 90-93] with unmodified samples in this study having fracture toughness values of 1.15±0.06 MPa·m$^{1/2}$. For 100W films, fracture toughness increases to 1.78±0.1 MPa·m$^{1/2}$ (55% increase).

5.5 Discussion

Fracture toughness is a material property that describes a material's innate ability to resist crack propagation. Experimentally, fracture toughness is determined by imparting a flaw in a sample, determining the location of crack initiation. In this study, flaws were imparted using a Vickers indenter in order to control flaw sizes and geometry. Observed critical flaw sizes are on the order of 73 microns and have a semicircular geometry, comparable to studies of fractured porcelain showing critical flaw sizes of 60-70µm for air-abraded porcelain samples.[94] Measured fracture toughness values in this study were 1.15±0.06 MPa·m$^{1/2}$ whereas literature values show porcelain fracture toughness to be approximately 1.0 MPa·m$^{1/2}$.[27, 90-93] By applying thin film YSZ coatings over the substrate surface, we achieved a 55% increase in fracture toughness over unmodified specimens.

Increases in fracture toughness may be attributed to three strengthening mechanisms; compressive film stresses, crack deflection, and flaw modification. Compressive film stresses arise as particle bombardment occurs during film growth.[95] During this process, kinetic energy of impinging atoms causes agglomeration of deposited atoms parallel to a substrate surface. As film growth continues, proximity of atoms induces lattice expansion; however, expansion is inhibited by neighboring atomic clusters. As a result, compressive stresses along this plane are generated, while expansion in the direction perpendicular to the substrate remains uninhibited. This mechanism has been used to describe typical columnar film morphology in physical vapor deposited (PVD) films.[54-55] In sputtered, YSZ thin films, films stresses induce a tetragonal to monoclinic phase transformation, allowing for a correlation between film stress and %monoclinic volume fraction.[57] Monoclinic volume fraction was then measured by comparing relative intensities of the Tetragonal ($I_{T(111)}$) and Monoclinic ($IM_{(111)}$) peaks.[59] With the application of a substrate bias during deposition, kinetic energy of impinging atoms are increased, resulting in increased film stresses and increased %monoclinic phase (Figure 1A).

As %monoclinic volume fraction is increased, film morphology shifts from a columnar structure (Figure 1B) towards an interrupted structure (Figure 1C), (characterized by lateral cracks) as a mechanism for film stress relief.[57] With a columnar structure, crack paths are expected to propagate through the straight, inter-columnar grain boundaries. However, presence of lateral defects may provide a crack deflection mechanism during failure. As cracks lengths are increased, fracture energy is increased, exhibited by an increase in fracture strength. Fracture surfaces of these interrupted microstructures show ledges (Figure 1C), indicating evidence for crack deflection during fracture.

Impinging atoms can preferentially fill cracks as they migrate across a surface, leading to an increase in local radius of curvature.[20] In this case, crack tips are blunted, increasing force required for crack propagation. Figure 2C shows adhesion of a deposited YSZ film over a Vickers indent. Crack tip blunting effects are inconclusive from SEM analysis. However, critical flaw characteristics can be determined, leading to insight regarding failure mechanisms. These flaws are shown to exhibit a standard, semi-circular shape, 63$\pm$1 μm in diameter (Figure 2B). Geometry of the Vickers indent can be seen with a corresponding damage zone immediately under the indent, in the substrate. It is expected that under flexure loading, fracture initiation occurs at the interface between this damage zone and the rest of the substrate. During fracture initiation, compressive stresses in the coatings resist crack propagation. Once this compressive stress is overcome by tensile loading conditions, crack propagation begins, resulting in critical flaw characteristics. Also during crack propagation, lateral cracking in interrupted microstructures will provide additional strengthening to the construct. Therefore compressive film stresses likely act as a primary strengthening mechanism whereas crack deflection acts as a secondary strengthening mechanism in this system.

Imparting flaws into a surface with an indenter allows for a method that produces consistent flaws, resulting in consistent fracture characteristics. As a result, fracture data is normalized for flaw size and geometry, leading to reduced error. As expected, fracture strength of samples modified by films are shown to be improved ($P \leq 0.05$) over substrates unmodified by a film (Figure 3). Due to film strengthening effects, increases in fracture strength of up to 55% can be observed with increasing substrate bias. While increasing substrate bias is expected to lead to further improvements in fracture strength, bias plasma becomes unstable and increased film stresses leads to delamination, reducing the effectiveness of films.

Combining critical flaw analysis and fracture strength data allows for calculation of fracture toughness values. Similar to fracture strength improvements, increases in fracture toughness of up to 55% can be observed with increasing substrate bias. In order to more accurately characterize the contributions of each mechanism to overall strength of the construct, the system must be modeled by analyzing stresses throughout the construct. It has been shown that stresses on a surface of cracks of this geometry can be effectively modeled.[43] By modifying models to consider a compressive coating over a semi-circular crack, contributions of strengthening of from film stress, crack deflection, and flaw modification of YSZ films on substrate can be quantified. This model may offer insight to the location of failure initiation, leading to more effective design and further strength improvements.

Data show support for the hypothesis for biased-YSZ coatings as an effective method for improving fracture toughness of dental porcelain by up to 55% over unmodified samples. Improvements are attributed to compressive stresses and modified film microstructures, which upon loading, act to resist crack propagation. Introduction of controlled flaws allows for future work to model and extrapolate strengthening effects on varying flaw sizes, geometries, and substrates. Increases in fracture toughness demonstrate YSZ coatings as a viable method for improving reliability of all-ceramic dental restorations.

5.6 Conclusion

Surface modification of dental ceramics with YSZ thin film coatings is shown as a viable method for improved reliability of dental ceramic materials. Increases in strength are correlated to increased compressive film stresses and modified YSZ microstructures. Future studies will evaluate clinically relevant constructs and a development of a thin film strengthening model. A 55% increase in overall apparent fracture strength can have significant ramifications on the longevity and reliability of all-ceramic restorations.

CHAPTER 6: A PREDICTIVE FRACTURE STRENGTH MODEL FOR BRITTLE SUBSTRATES UNDER THE INFLUENCE OF YTTRIA-STABILIZED ZIRCONIA (YSZ) THIN-FILM RESIDUAL STRESSES

To be submitted to the Journal of Dental Materials

Running title: Modeling the effect of thin-film residual stresses on brittle substrates

Running Authors: Chan et al.

Ryan N. Chan

North Carolina State University, Department of Materials Science and Engineering, 911 Partner's Way, EB1 Room 3002, Raleigh North Carolina 27695 and RTI International, Center for Materials and Electronic Technologies, PO Box 12194, 3040 Cornwallis Rd. RTP, North Carolina 27709

Brian R. Stoner

RTI International, Center for Materials and Electronic Technologies, PO Box 12194, 3040 Cornwallis Rd. RTP, North Carolina 27709

Ronald O. Scattergood

North Carolina State University, Department of Materials Science and Engineering, 911 Partner's Way, EB1 Room 3002, Raleigh North Carolina 27695

Jeffrey Y. Thompson

Nova Southeastern University, Section of Prosthodontics, 3301 College Avenue, Fort Lauderdale, Florida 33328

Jeffrey R. Piascik

RTI International, Center for Materials and Electronic Technologies, PO Box 12194, 3040 Cornwallis Rd. RTP, North Carolina 27709 and North Carolina State University, Department of Materials Science and Engineering, 911 Partner's Way, EB1 Room 3002, Raleigh North Carolina 27695

6.1 Abstract

The versatile properties of all-ceramic dental restorations including biocompatibility aesthetics have promoted their use over comparable metal restorations. However these properties come at a sacrifice of crack resistance properties found in more mechanically robust materials systems. Analysis of clinically failed all-ceramic specimens observed failure initiation on the inner surface of restorations, where tensile stresses and surface flaws were found to accelerate construct failure. Here, a Vickers indenter was used to induce consistent failure by imparting a critical flaw (40-100μm) with controlled size and shape into ProCAD (Ivoclar-Vivadent) bar specimens (2x2x18mm, n=30). Indented surfaces were then coated with 2μm of Yttria-stabilized zirconia (YSZ) via radio frequency magnetron sputtering (30:1 Ar/O_2 gas ratio) where compressive film stresses have been shown to increase construct fracture strength. Depositions were performed with varying powers of substrate bias (0-100W) and construct flexural strength was determined by three-point bend testing. Fractography and Weibull analysis was used to determine delineate multiple fracture mechanisms. Fracture strength data showed strength improvements of up to 53% attributed to compressive surface stresses. Fractography showed subsurface failure initiation despite imparted critical flaws. Data was then used to develop a force model to quantitatively determine the contribution of compressive YSZ thin-film forces on increased construct fracture strength.

6.2 Introduction:

All-ceramic materials have been highly coveted for dental restoration applications due to their biocompatibility and esthetic properties.[46, 80-83, 96-97] Of the all-ceramic materials, aesthetic versatility and machinability properties of glass ceramics (porcelain) have resulted in their extensive use in dental restorations.[49, 83, 98] However, ceramics under tensile loading are ineffective against crack propagation and tensile stresses.[49, 92] Analysis of clinically failed all-ceramic restorations have shown that the majority of failures originate on the interior side, where flexure induced stresses have been shown to arise from forces associated with mastication.[46, 96, 99] This study aims to show a viable method for improvements in fracture behavior of dental ceramic constructs (porcelain) by depositing a thin, compressively stressed yttria-stabilized zirconia (YSZ) films. Additionally, a simplistic model of strengthening mechanisms is introduced to assist in predicting fracture behavior improvements.

Despite porcelain's widespread use, its low fracture strength has impeded its continued growth as a universal dental ceramic. Fracture strength of these brittle materials typically are characterized by an elliptical, initial flaw surrounded by a larger, elliptical area that designates the flaw size.[15-16] According to ceramic fracture toughness principles, material strength is dictated by size and geometry of a critical flaw. Clinical dental restorations are typically etched or air abraded on the inside of a restoration to improved adhesion. These clinical procedures increase surface area for improved bonding to dental resins; however, these techniques induce large surface flaws, increasing the number of potential critical flaw initiators and the chance of premature failure.[12-14]

Fracture surfaces of specimens can be analyzed to reveal these characteristics so that comparisons can be made between specimens to determine information such as stresses related to failure.[16, 96, 100-101] These data have helped derive methods used to impart compressive residual stresses on a surface to increase material strength. For example, thermal and tempered glass systems have been studied extensively. Here thermal processing techniques are used to induce a compressive surface layer to inhibit surface flaw initiation and propagation.[102-104] However, roughening techniques relieve surface stresses, causing an inherent residual stress to be less practical in application. Similarly, thermal treatments to dental materials are used to treat coatings and glazes so that upon curing, they exist in a compressive state.[50, 105] Ruddell et al. has shown an alternative to thermal treatments by depositing a compressive metallic thin film on ceramic substrates via radiofrequency (r.f) magnetron sputtering.[20] Mechanical testing revealed improvements in fracture strength of up to 19% with less than 10μm of thin film. Earlier work also reported up to a 32% increase in fracture strength by using a multilayer film (10 μm) structure consisting of alternating layers of yttria-stabilized zirconia (YSZ) (1 μm) and parylene (1 μm).[23] Additionally, it was determined that a 2-3 μm thick YSZ thin film sputtered on porcelain substrates provide the maximum benefit for increased construct fracture strength.[21] Further work showed an ability to control sputtered, YSZ film stresses by varying parameters during deposition.[22, 57-58]

Utilizing these techniques of depositing YSZ on a dental porcelain with controlled flaws, fracture strength and fracture toughness improvements of up to 55% were observed.[106] Primary strengthening mechanisms were attributed to YSZ compressive stresses. Here, we the effect of compressive YSZ films on varying flaw sizes and a predictive model to quantify film forces acting on a critical flaw is introduced.

6.3 Method and Materials:

A low-speed saw (Buehler Isomet, Lake Bluff, Illinois) was used to cut 18 x 2 x 2 mm specimens from leucite-reinforced feldspathic porcelain blocks (ProCAD, Ivoclar-Vivadent, Schaan, Liechtenstein). A wet polishing wheel (Allied, Rancho Dominguez, California) was used with 250 through 1200 grit SiC abrasive (Allied, Rancho Dominguez, California) at 200RPM to polish the four large surfaces of each specimen. Specimen edges were then rounded using 1200 grit SiC abrasive at 100RPM to limit corner and edge failures. Substrates were ultrasonically cleaned in acetone the deionized water to remove surface debris prior to deposition and randomly divided into groups (n=30).

In order to normalize failures through control of critical flaw size and geometry a single, a Vickers indenter (Mitutoyo Model AAV-500, Aurora, IL) was used to impart an indentation into the center of a substrate surface with indent corners perpendicular to substrate edges. Loads of 0.3, 0.5, and 1N were applied with a load time of 15 seconds, resulting in flaw sizes of 40, 70, and 100μm, respectively. Indent sizes and crack lengths were measured using an optical microscope (Sony DXC-390, Exwave HAD, Irvine, California) prior and post thin-film deposition to ensure flaw uniformity during fracture.

All specimens were coated with 2μm of YSZ thin-film to maximize fracture strength.[21] Thin-film coatings were performed using r.f. magnetron sputtering (CVC Model SC-400, Rochester, NY). Target material used for sputtering was 99.99% pure zirconia doped with 3mol% yttria (Plasmaterials, Livermore, CA). Substrates were mounted at a working distance of 75 mm, with the indented surface exposed to the target. For samples requiring substrate bias, a second r.f. power source was capacitively coupled to the substrate. To promote film adhesion, a 50W substrate bias in 30:1 argon to oxygen atmosphere was applied for 5 minutes to clean organic debris from specimen surfaces prior to deposition. All depositions were performed with a target power of 350 W, atmosphere of 30:1 argon to oxygen, and substrate bias varied between 0 and 100 W.

Flexural testing (Instron Model 5542, Norwood, MA) was conducted using a three-point bending fixture, with specimens oriented with films in tension per ASTM Standard C1161.[63] Testing conditions featured a 10 mm span and a crosshead speed of 0.5 mm/min. Bar dimensions were measured prior to fracture for fracture stress calculations. Peak loads and fracture stresses for each specimen were recorded for sample sizes of n=30. At each flaw size, a polished sample set with a Vickers indentation was left unmodified by films to act as a control group. Fracture analysis was performed using scanning electron microscopy (SEM) (Hitachi, S-4700 FE, Tokyo, Japan) and optical microscopy (Sony DXC-390, Exwave HAD, Irvine, California) were used to characterize specimen fracture surfaces.

6.4 Results:

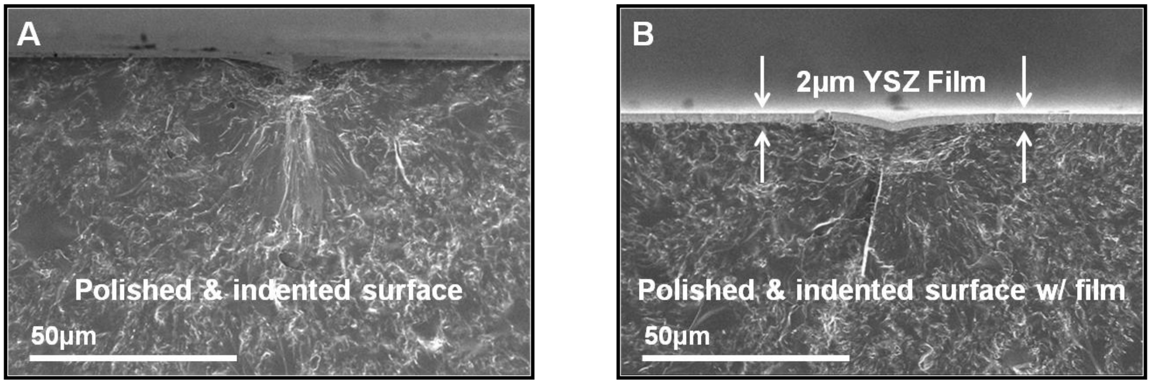

Figure 6.1: (a) SEM image of a fracture surface from a polished specimen where critical flaws are shown to originate from the location of Vickers indentation. (b) SEM image of a fracture surface from a polished and coated specimen where similar critical flaw features are observed and thin-films are shown to conform to indent shape.

A Vickers indenter was used to impart a singular critical flaw in a polished surface of each specimen to control critical flaw geometry and location. Specimens were loaded under 3-point bend flexure with imparted flaws located on the specimen's tensile surface. Fracture analysis showed that fracture consistently occurred at the location of the imparted flaws (Figure 6.1A). In order to analyze the benefits of compressive YSZ thin-films, it was critical to ensure thin-film-substrate adhesion. All specimens were subjected to a Ar/O_2 surface plasma prior to deposition to physically clean and chemically functionalized the surfaces. Fracture surface analysis of film-substrate constructs displayed thin-film conformation and similar flaw-failure characteristics as compared to non-coated control specimens at the location of indentation (Figure 1B).

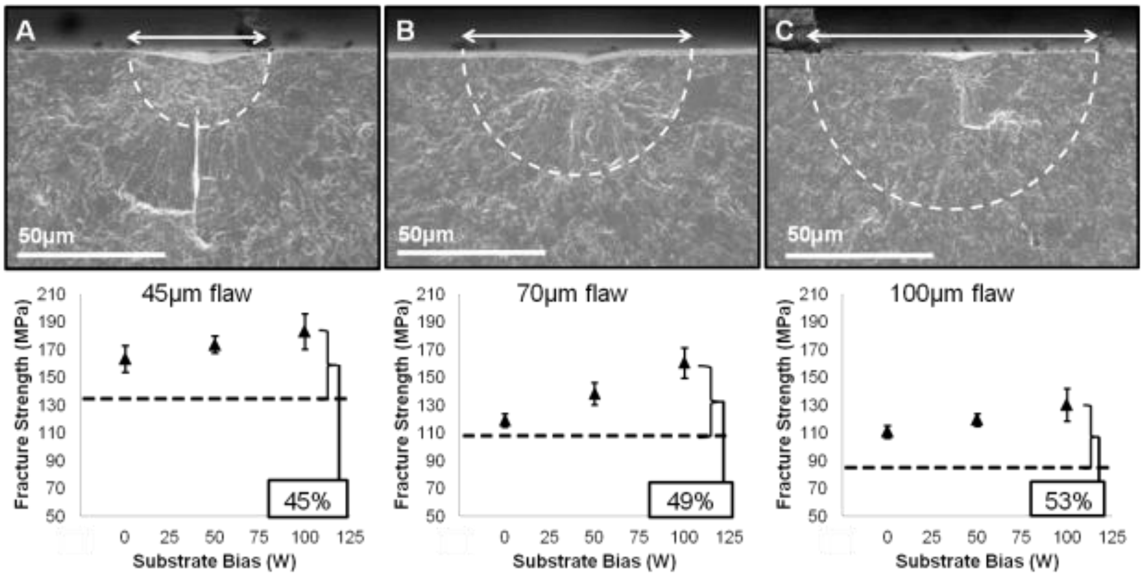

Figure 6.2: SEM images of fracture surfaces show fracture characteristics on an (A) 45μm flaw, (B) 70μm flaw, and (C) 100μm flaw. Graphs show corresponding fracture strength data where dotted lines represent strength of uncoated control specimens, and plotted data represents strength of YSZ thin-film modified specimens with varied substrate bias during deposition.

Specimens were prepared by imparting flaw sizes of 45, 70, and 100μm into substrate surfaces prior to coating with YSZ thin-films. YSZ thin-films were deposited by altering substrate bias (0, 50, 100W) during deposition to produce varying magnitudes of compressive film stress.[106] As expected, fracture strength was observed to increase with a decreasing flaw size. Maximum fracture strength improvements of 53% were observed relative to uncoated samples.

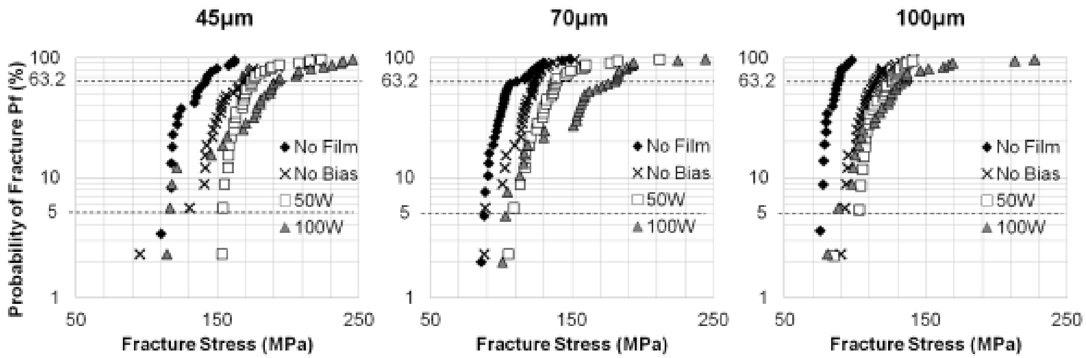

Figure 6.3: *Graphs show probability of failure on a semi-log plot for all fractured specimens. Dotted lines represent 63.2% probability of failure (characteristic strength) and 5% probability of failure. Relative to uncoated specimens, shift in data with increased substrate bias indicates an increase in apparent fracture strength.*

Weibull analysis was conducted to show statistical distributions of probability of failure for fractured samples. Data show reduced probability of fracture with decreasing flaw size and increasing substrate bias during deposition (Figure 6.3). For each flaw size, specimens with film are compared to uncoated specimens. A shift in characteristic strength (defined by fracture stress at 63.2% probability failure) indicates increased strength of coated samples ranging from 12-45% (Table 6.1). Slope shifts within a sample are also observed, indicating change in active failure mechanism.

Table 6.1: Characteristic strength (fracture stress at 63.2% probability failure) and % increase in strength for fractured groups with varying flaw size and coating conditions.

	45µm		70µm		100µm	
	Characteristic Strength (MPa)	**% Strength Increase**	**Characteristic Strength (MPa)**	**% Strength Increase**	**Characteristic Strength (MPa)**	**% Strength Increase**
No Film	129.4	n/a	102.8	n/a	83.2	n/a
No Bias	156.2	20.7	115.4	12.3	107.1	28.8
50W	167.8	29.6	131.1	27.6	116.3	39.9
100W	170.6	31.8	149.0	45.0	119.6	43.8

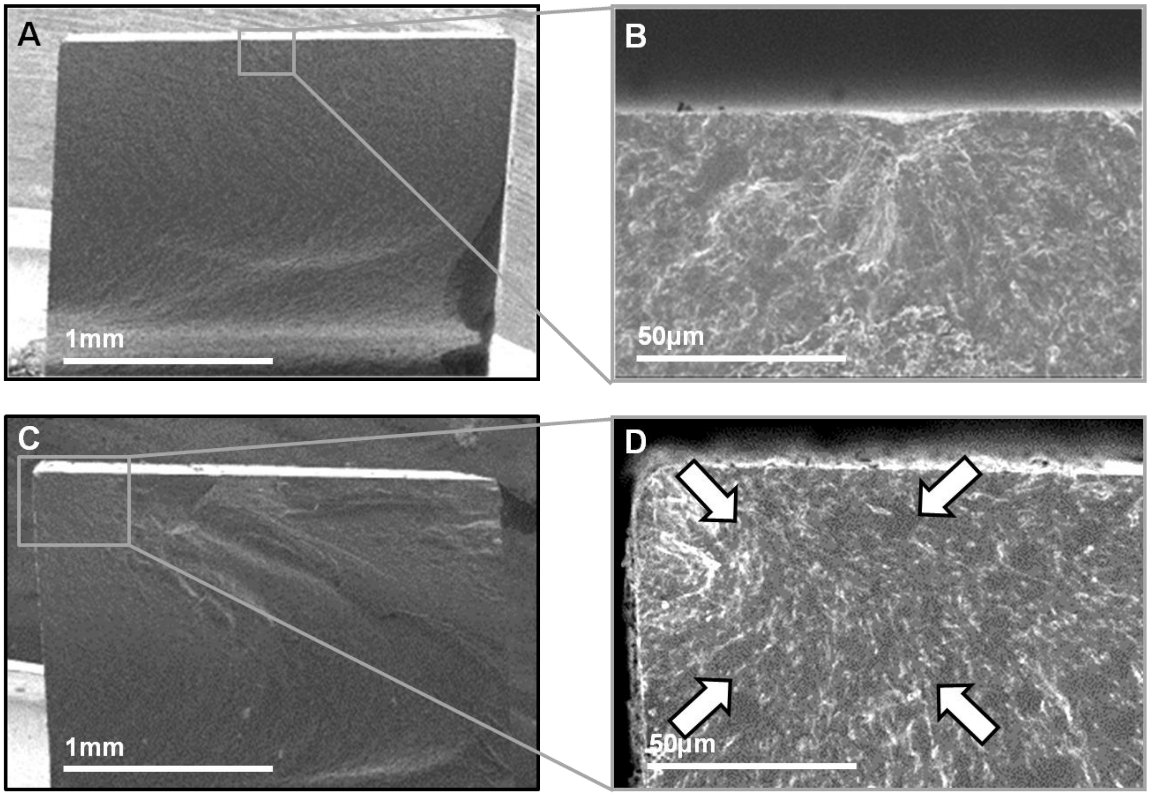

Figure 6.4: SEM images showing a typical brittle fracture surface (A) with failure origin at the location of the imparted Vickers indentation (B) and an atypical fracture surface (C) indicative of crack deflection, with subsurface failure origin (D).

Fractography was used to categorize failure surfaces according to active flaw types. Typical brittle failure is observed in all uncoated specimens, categorized by smooth fracture surfaces (Figure 6.4A). Upon magnified examination, failures were shown to originate from the location of Vickers indentation (Figure 6.4B). Failure surface analysis of select coated samples show more textured surfaces (Figure 6.4C), and failure initiation from a subsurface flaw, away from the indent location (Figure 6.4D). Subsurface failures correspond to decreased Weibull slopes and increased fracture strengths.

6.5 Discussion:

In order to normalize fracture, a Vickers indenter was used to impart a controlled flaw into a polished surface of each specimen. By creating a sharp notch and residual damage zone from indentation, this method can be used to more precisely control the location of failure. Furthermore, by imparting flaws with controlled size into a polished surface, fracture strengths and failure modes are normalized in each specimen. Prior to deposition, surfaces were subjected to low-energy argon plasma to clean surfaces from organic debris. As reported by Knotek et al., exposure to plasma can induce ion bombardment and interrupt surface Si-O-Si bonding.[95, 107] Surfaces were then coated with 2μm of YSZ thin-film where Zr^{4+} ions can chemically bond to available O^{2-} sites. Induced chemical adhesion at the YSZ-porcelain interface will therefore provide a more reliable construct compared to less reactive surfaces. It is observed that films conform well to the indenter flaw geometry and did not delaminate during fracture, indicating good thin-film adhesion (Figure 6.1b).

Earlier work using compressive YSZ thin films on an induced flaw reported that using substrate bias increased apparent fracture toughness up to 51% over unmodified substrates.[106] By varying substrate bias during deposition, it was observed that thin-film compressive stresses correlated to an increased volume% of Tetragonal to Monoclinic phase transformation which ranged from 50-84%. During this process, an applied substrate bias during deposition increases kinetic energy of impinging ions during particle bombardment. As ion bombardment is increased, film densification occurs. However, lateral expansion is inhibited due to proximity of neighboring grains and as a result, compressive film stresses are increased. These compressive stresses introduce a barrier to fracture by resisting tensile forces under flexure. As a result, construct fracture strength is increased.[106]

Here, fracture strength improvements were measured as substrate bias during deposition and flaw sizes are varied. By selecting multiple flaw sizes (45, 70, 100μm), a model can be developed to describe the relation of effect of compressive YSZ film stresses bulk mechanical properties of the film-substrate construct. It was observed that similar fracture strength increases occurs independent of flaw size. Specimens with films deposited without a substrate bias (0W) during deposition show a moderate improvement in strength over non coated specimens. For all flaw sizes, maximum strengthening is observed with the film deposited with the highest substrate bias (100W). It is expected that further increases in fracture strength should be observed; however unstable deposition parameters and delamination begin to occur if compressive stresses are increased beyond the YSZ-porcelain interfacial strength.

Fracture surface analysis shows that fracture characteristics of induced flaws are similar in size and pattern to clinically reported failures[46, 96], despite varied flaw size (Figure 6.2). As evidenced by Weibull analysis, multiple mechanisms contributing to failure are likely active in the selected samples. Typical brittle failures are observed in all no film specimens (Figure 6.4A). These fracture surfaces are characterized by their smooth surfaces, indicative of fast, catastrophic failure. It is also observed that all specimens within the non-coated sample group exhibit failure origins from the indent location. In contrast, specimens coated with 50W bias film can be categorized by fracture behavior into two groups. Lower strength, coated specimens exhibit similar fracture characteristics to uncoated specimens (smooth fracture surface and failure origins at the indent). However, higher strength, coated specimens exhibit a more textured fracture surface, indicative of crack deflection. Furthermore, failure origins are no longer at the indent location and instead observed at subsurface defects away from the indent. As indicated by Weibull analysis, a transition in active flaw mechanism is expected with higher strength specimens.

As described by the weakest link theory of ceramic fracture[108], probability of failure at a given load is based flaw distribution. Therefore, when failure at the indent location is overcome by compressive residual stresses, a new weakest link becomes the new failure origin. Rationale for subsurface failure is supported by residual stress studies that describe a subsurface tensile region a given depth into a specimen as compressive surface stresses are introduced.[109] These tensile stresses may contribute to the subsurface failure origins, as observed by fractography in high strength, coated specimens (Figure 4D).

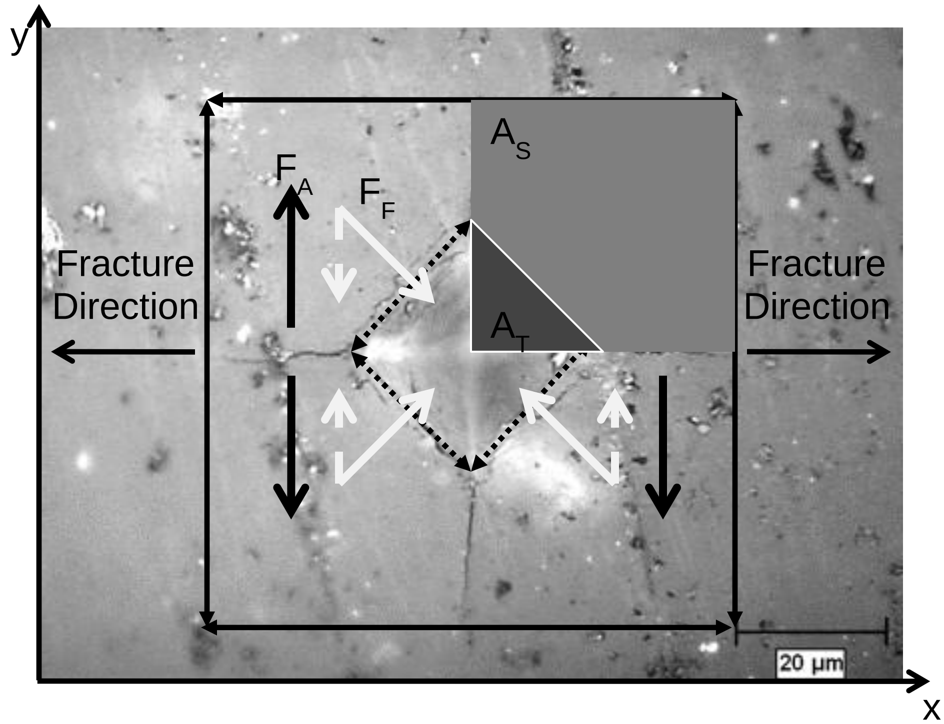

Figure 6.5: Optical image of an indented surface is overlaid with analyzed areas and force vectors

Fracture strength data was used to develop a model to describe the behavior of compressive film stresses and quantified forces over an induced surface flaw (Figure 5A). In this model, the analyzed area is defined by radial crack length (critical flaw size). Analyzed area is broken into 4 quadrants where in each quadrant, film stress direction is towards the center of indent. The model assumes that film stresses are the dominant strengthening mechanism and are uniform over the modeled area. Furthermore, under uniaxial loading, only forces in the y-direction will contribute towards fracture and strengthening. Therefore at fracture, the fracture stress is equivalent to the sum of inherent strength of a specimen and compressive forces from the deposited YSZ film.

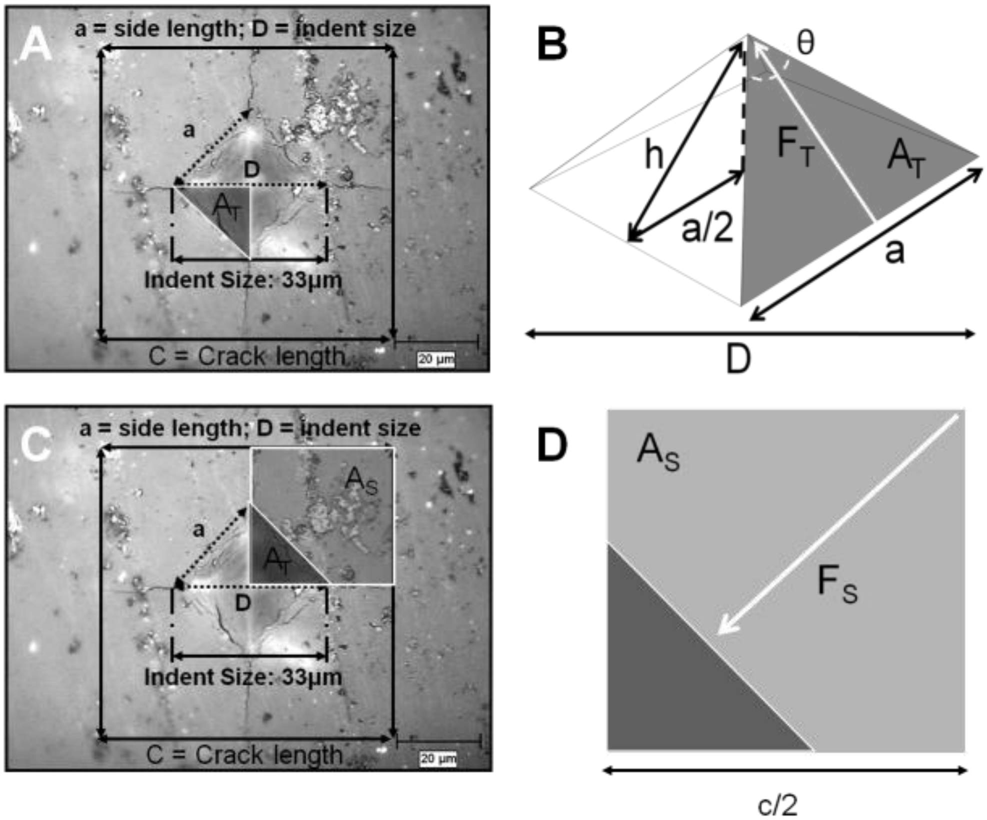

Figure 6.6: *An optical image showing (A) analyzed areas and defined parameters of the internal areas of a Vickers indent, (B) a model showing the 3D structure of the indent volume, (C) analyzed areas and defined parameters of the surface area around a critical flaw, and (D) a model showing the force vectors on the surface of a critical flaw.*

6.5.1 Triangular Area Calculations:

Critical flaw area is split into four quadrants with force vectors directed towards the center of the indent. Each quadrant area is subdivided into two areas; a triangular area representing ¼ of the indent (Figure 6A: A_T) and a square area with A_T subtracted (Figure 6.6C: A_S). Optical images are used to measure indent size (D), which given Vickers indenter geometry (Angle between faces, θ=136°), can be used to calculate film force contributions as follows (Figure 6.6B):

$$\text{Side length, a} = \frac{D}{\sqrt{2}} \qquad \text{Eq. [6.1]}$$

$$\text{Triangular height, h} = \frac{a/_2}{\tan\theta/_2} \qquad \text{Eq. [6.2]}$$

$$\text{Triangular Area, } A_T = \frac{1}{2} \cdot a \cdot h \qquad \text{Eq. [6.3]}$$

$$\text{Film stress, } \sigma = \frac{F_T}{A_T} \qquad \text{Eq. [6.4]}$$

$$\text{So that force over the triangular area, } F_T = \sigma \cdot A_T \qquad \text{Eq. [6.5]}$$

Because we assume that under flexural loading, tensile stresses are maximized on the surface and that stresses point towards the center of the indent, we must calculate the 2-dimansional surface force component of the 3-dimensional force vector.

$$\text{Angle of indent } \theta' = \cos^{-1}\left(\frac{a/_2}{h}\right) \qquad \text{Eq. [6.6]}$$

$$\text{2-dimensional surface component of force, } F_T' = F_T \cdot \cos\theta' \qquad \text{Eq. [6.7]}$$

Because we assume that under 3point flexural loading, stresses are uniaxial, we calculate the y-component of the 2-dimensional surface force vector.

Y-component of the 2-dimensional surface force, $F_{yT}^{'} = F_T^{'} \cdot \sqrt{2}$ Eq. [6.8]

For the sum of all uniaxial surface forces, total F_T force over $A_T = 4 \cdot F_{yT}^{'}$ Eq. [6.9]

6.5.2 Square Area Calculations:

Total Force over square area is calculated as follows (Figure 6.6D):

Area of square with triangular cutout, $A_S = (\frac{c}{2})^2 - \frac{1}{2} \cdot \frac{D}{2} \cdot \frac{D}{2}$ Eq. [6.10]

Simplified to $A_s = \frac{c^2}{4} - \frac{D^2}{8}$ Eq. [6.11]

Film stress, $\sigma = \frac{F_S}{A_S}$ Eq. [6.12]

So that force over the square area, $F_S = \sigma \cdot A_S$ Eq. [6.13]

Since this is already a surface force, there is no need to calculate the 2-dimensional force component. However, the y-component of F_S must still be calculated:

Force in y-direction, $F_{yS} = \frac{F_S}{\sqrt{2}}$ Eq. [6.14]

For the sum of all uniaxial surface forces over the square area, total F_S force over A_s

$A_S = 4 \cdot F_{yS}$ Eq. [6.15]

For the sum of all uniaxial surface film forces over the total area,

$F_F = 4 \cdot F_{yT}^{'} + 4 \cdot F_{yS}$ Eq. [6.16]

6.5.3 Total Film Force on Flaw:

In this model, the difference in force between control samples and samples modified by films is calculated. Total forces in the system are assumed to be at equilibrium at failures:

$$\sum F = F_I + F_F + F_A = 0 \qquad \text{Eq. [6.17]}$$

Where an applied load induces a tensile force (F_A) which is resisted by the compressive, inherent strength of the material (F_I), and compressive film force (F_F) so that

$$F_A = F_I + F_F \qquad [6.18]$$

For the condition of no film in control samples, film force is zero (F_F=0) so that

$$F_A = F_I \qquad [6.19]$$

In this condition, the applied load at fracture is measured from flexure testing and used to calculate the intrinsic resistance strength of the material (F_I). Intrinsic strength is then assumed to be the same for all samples so that film forces can be calculated from equation 6.18.

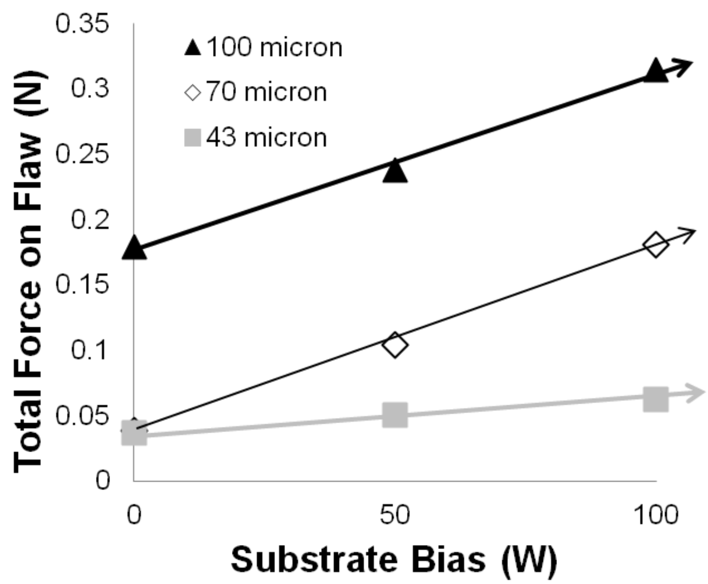

Figure 6.7: *Forces on a critical flaw were calculated based on model given flaw size, flaw geometry and fracture strengths for samples with varying flaw sizes and film stresses.*

As measured fracture strength increases, the difference in fracture strength over uncoated samples is used to calculate total force over the area of an induced surface flaw. As also evidenced by fracture strength testing, forces on a critical flaw are increased as substrate bias is increased. Total force on a flaw also increases with flaw size, due to the increased area over which the film-substrate interaction is considered. Given flaw size and geometry, these forces can be inserted into equations 6.4 and 6.12 with a given flaw area to calculate an approximate film stress. It was observed that these approximate film stress calculations follow closely with measured film stresses (Figure 6.8).[57]

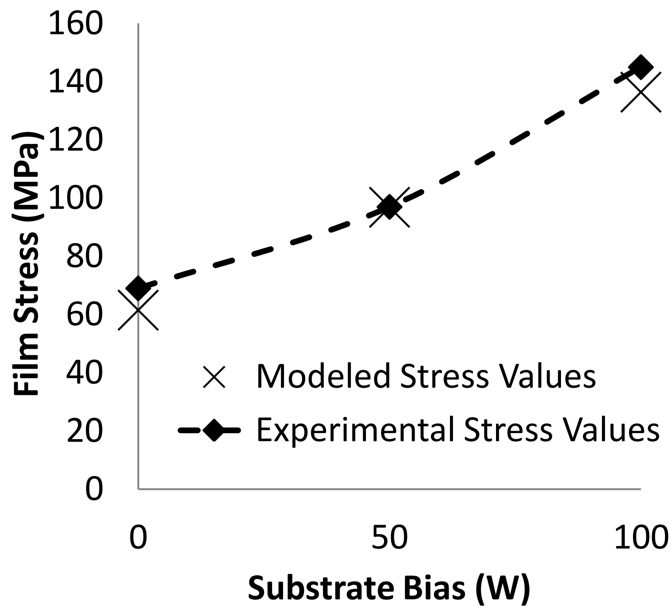

Figure 6.8: When compared to experimental film stress measurements, modeled film stress values were observed to compare closely in magnitude.

It can be concluded that for film-substrate constructs, when flaw characteristics and construct mechanical properties are known, this empirical model may be used to estimate film stresses where direct film measurements may not be practical. Furthermore, when given film stresses in addition to flaw characteristics, this model may serve as an estimate of construct fracture strength for complex components with surface stress gradients.

6.6 Summary:

Increases in fracture behavior are observed on varied flaw sizes. Weibull analysis indicates dual fracture mechanisms during failure. Fractography confirms multiple failure mechanisms with subsurface failure initiation becoming the dominant mechanism when compressive film stresses are increased. Compressive stresses prevent fracture from occurring at surface, and subsurface flaws become active flaws. A model to estimate total forces on a critical flaw has been developed which can be used to empirically estimate specimen fracture strength given residual surface stress, flaw size and flaw geometry.

CHAPTER 7: SUMMARY, CONCLUSIONS, AND SUGGESTIONS FOR FUTURE WORK

This work aimed to study the mechanical properties of PSZ-altered ceramic constructs and to demonstrate viable techniques for improving the longevity and reliability of all-ceramic dental restorations. It was determined that applying a compressive, thin-film coating to all-ceramic substrates, provides strength advantages over current, clinical preparation methods. Analysis of fracture constructs via Fractography and Weibull analysis indicate significant increased fracture energy compared to that of uncoated specimens. By developing a associated models for thin-film-ceramic constructs this work provides quantitative analysis of compressive thin-film forces, based on associated strengthening mechanisms. Furthermore, multiple fracture testing methods and flaw conditions suggest YSZ coating may be expanded to strengthening brittle materials in other applications where temperature or wear resistance and/or biocompatibility are required.

7.1 Microstructural effects on fracture strength of yttria-stabilized zirconia (YSZ) thin-film modified constructs

YSZ thin-films were deposited with varying microstructures on silicon wafers and dental porcelain by r.f. magnetron sputtering. While thicker films provide compressive forces on a critical flaw, columnar microstructures are thought to be non ideal due to their instability in aqueous environments. By applying a substrate bias during deposition, thicker films can be grown with zone 1, or disrupted microstructures. Control of these microstructures would therefore allow for film stresses and potentially other properties to be tailored to applications independent of film thickness.

Data from biaxial flexure suggest an increasing trend in fracture strength with increased substrate bias. This strengthening effect is attributed to resistance of crack expansion via forces in the film, which exert compressive forces on a substrate surface. A qualitative, fractography analysis of fractured specimens suggests an increasing trend in fracture energy versus substrate bias, supporting the ability to strengthen ceramic substrates with bias-assisted sputtered YSZ films. Further studies may work to reduce sample scatter and to further develop a structure-property model for the effect of compressive film stresses on the flexural strength of a ceramic construct.

7.2 Fracture toughness improvements on dental ceramic through use of yttria-stabilized zirconia (YSZ) thin-film coatings

Surface modification of dental ceramics with YSZ thin film coatings is shown as a viable method for improved reliability of dental ceramic materials. Increases in strength are correlated to increased compressive film stresses and modified YSZ microstructures. Future studies will evaluate clinically relevant constructs and a development of a thin film strengthening model. A 55% increase in overall apparent fracture strength can have significant ramifications on the longevity and reliability of all-ceramic restorations.

7.3 A predictive fracture strength model for brittle substrates under the influence of yttria-stabilized zirconia (YSZ) thin-film residual stresses

Increases in fracture behavior are observed on varied flaw sizes. Weibull analysis indicates dual fracture mechanisms during failure. Fractography confirms multiple failure mechanisms with subsurface failure initiation becoming the dominant mechanism when compressive film stresses are increased. Compressive stresses prevent fracture from occurring at surface, and subsurface flaws become active flaws. A model to estimate total forces on a critical flaw has been developed which can be used to empirically estimate specimen fracture strength given residual surface stress, flaw size and flaw geometry.

7.4 Suggestions for Future Work

Although evidence for improved fracture behavior is provided, this work primarily focused on simple surface conditions (roughened, polished, and singular controlled surface flaws). Analysis of complex surface conditions including multiple flaw sites, or varying degrees of surface roughness may provide further insight to the lifetime and reliability of a YSZ thin film modified surface. From a mechanistic view, interfacial modifications from ion bombardment are cited as a mechanism for construct strengthening. This technique is hypothesized to provide improved surface reactivity due to exposure of surface oxygen atoms and its affinity for binding to zirconia (Figure 7.2). Improvements to interfacial adhesion, are expected to allow for increasing film stresses to be applied with mitigated risk for delamination.

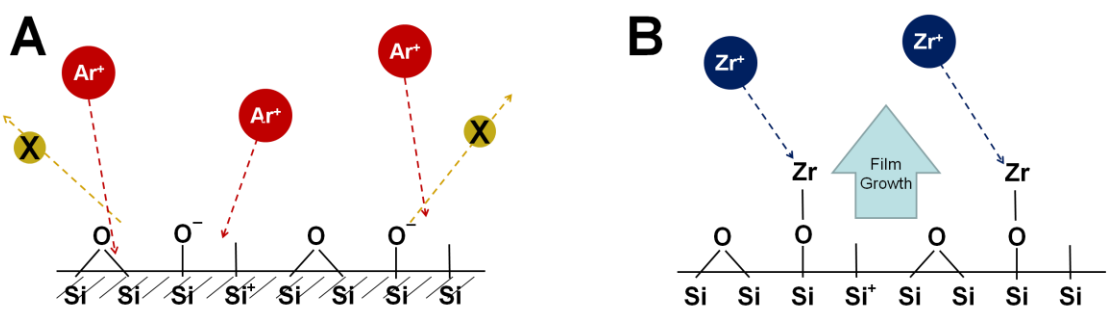

Figure 7.1: A proposed mechanism for improved thin film adhesion through substrate exposure to and Oxygen/Argon plasma. (A) Argon atoms bombard surfaces, removing organic debris and destroying Si-O-Si bonds. (B) Dangling O bonds are free to combine with to sputtered Zr ions, resulting in a chemical bond.

Additionally, while this work showed increases to fracture strength and fracture toughness, further work is needed to conclude a long-tem benefit to mechanical properties. Cyclic loading (fatigue testing) or varied loading rates (dynamic fatigue) may provide further insight to long term reliability of thin-film modified constructs. Furthermore, much remains to be discovered surrounding the strengthening mechanisms involved in this system. Finite element analysis (FEA) may be used to understand the effect of compressive surfaces on a singular critical flaw. To date, FEA studies have been conducted on stress fields surrounding an indentation and using indentation techniques to measure residual surface stresses. However analysis stress fields with varying degrees of interfacial or gradient residual stresses may allow for new preparation techniques to be implemented. Alternatively, one suggestion involves placing multiple Vickers indentations across a sample surface, and spaced such that the residual stresses from each indent do not interfere with one another. Upon fracture via 4-point loading, radial crack extensions of non critical flaws can be measured and compared to initial crack lengths. Changes in crack extension as distance is varied from a critical flaw would suggest similar data to FEA analysis.

Progressing and implementing these techniques into may lead to further versatility, longevity, and reliability improvements of all-ceramic dental restorations. More generally, this work may be expanded to other engineering systems where conventional strengthening techniques may not be applicable. For example in turbine applications, thin-film coatings may provide a low-profile strengthening technique where small tolerance windows do not allow for more macroscopic structural adjustments. Additionally, thermal and wear resistance of YSZ thin-film coatings can provide further improvements to component design, allowing for improved reliability, tolerance for harsh conditions, and/or efficiency of overall systems.

REFERENCES

[1] A. Sheiham, (2005). Oral health, general health and quality of life. *Bulletin of the World Health Organization*, 83(9), 644.

[2] C.A. Geissler, and J.F. Bates, (1984). The nutritional effects of tooth loss. *The American Journal of Clinical Nutrition*, 39(3), 478.

[3] Frost & Sullivan, (2008). U.S. Dental Implants Market. Report # N495-54.

[4] Marketsandmarkets.com, (2013). Dental Implants & Prosthetics Market (Implants, Crowns & Bridges, Dentures, Abutments) Current Tends, Opportunities & Global Forecasts to 2018. Report # MD 2129

[5] J.F. McCabe, and A.W.G. Walls, (2008). Chapter: 1 Science of Dental Materials. *Applied Dental Materials* (9th Edition). Oxford, UK: Blackwell Publishing Ltd.

[6] B.D. Ratner, A.S. Hoffman, F.J. Schoen, and J.E. Lemons, (2004).Chapter 2: Degradation of Materials in the Biological Environment. Biomaterials Science (2nd edition). San Diego, CA: Elsevier Academic Press.

[7] A. Shenoy, and N. Shenoy, (2010). Dental Ceramics: An Update. *The Journal of Conservative Dentistry*, 13(4), 195.

[8] E. Josefesson, R. Lindsten, and L.R.M. Hallberg, (2010). A qualitative study of the influence of poor dental aesthetics on the lives of young adults. *Acta Odontologica Scandinavica*, 68(1), 19.

[9] C. Flores-Mir, E. Silva, M.I. Barriga, M.O. Lagravere, and P.W. Major, (2004). Lay Person's perception of smile aesthetics in dental and facial views. *Journal of Orthodontics*, 31(3), 204.

[10] M. Freedman, F. Quinn, and M. O'Sullivan, (2007). Single unit CAD/CAM restorations: a literature review. *Journal of the Irish Dental Association*, 53(1), 38

[11] World Health Organization Report. (2009), Future Use of Materials for Dental Restoration: Report of the meeting convened at WHO HQ, Geneva Switzerland. Report # WU 190.

[12] N. De Jager, A. J. Feilzer, and C. L. Davidson, (2000). The influence of surface roughness on porcelain strength. *Dental Materials*, *16(6),* 381.

[13] A. R. Curtis, A. J. Wright, and G. J. P. Fleming, (2006). The influence of surface modification techniques on the performance of a Y-TZP dental ceramic, *Journal of Dentistry*. 34(30), 195.

[14] B. R. Lawn, B. J. Hockey, and S. M. Weiderhorn, (1980). Atomically sharp cracks in brittle solids: an electron microscopy study, *Journal of Materials Science*. 15(5), 1207.

[15] J. J. Mecholsky, R. W. Rice, and S. W. Freiman, (1974). Prediction of Fracture Energy and Flaw Size in Glasses from Measurements of Mirror Size, *Journal of the American Ceramic Society*. 57(10), 440.

[16] J.J. Mecholsky, (1995). Fractography: Determining the sites of fracture initiation, *Dental Materials*. 11(2), 113.

[17] S. M. Rekhson, (1993) Thermal Stresses Relaxation and Hysteresis in Glass, *Glass Sci. Technol.* 76(5), 1113.

[18] O. S. Narayanaswamy, (1978). Stress and Structural Relaxation in Tempering Glass, *Journal of the American Ceramic Society*. 61(3), 146.

[19] A. Xing Z. Jun, H. Chuanzhen, and Z. Jianhua, (1998). Development of an advanced ceramic tool material - functionally gradient cutting ceramics, *Materials Science and Engineering A*, 248(1) 245.

[20] D. Ruddell, J. Y. Thompson, and B. R. Stoner, (2000). Mechanical properties of dental ceramic coated by RF magnetron sputtering, *Journal of Biomedical Research, 51(3),* 316.

[21] E. C. Teixeria, J. R. Piascik, B. R. Stoner, and J. Y. Thompson, (2007). Effect of YSZ thin film coating thickness on the strength of a ceramic substrate, *Journal of Biomedical Research B, 83(2),* 459.

[22] D. Ruddell, B. R. Stoner, and J. Y. Thompson, (2003). The effect of deposition parameters on the properties of yttria-stabilized zirconia thin films, *Thin Solid Films 445*(1), 14.

[23] E. C. Teixeira, J. R. Piascik, B. R. Stoner, and J. Y Thompson, (2009). Zirconia–parylene multilayer thin films for enhanced fracture resistance of dental ceramics, *Proceedings of the institution of mechanical engineers part c-journal of mechanical engineering science, 223(7),* 897.

[24] A.A. Griffith, (1920). The Phenomena of Rupture and Flow in Solids, *Philosophical Transactions of the Royal Society of London. Series A, Containing Papers of a Mathematical or Physical Character*, 221(582), 163.

[25] GR Irwin, (1957). Analysis of Stresses and Strains Near the End of a Crack Traversing a Plate, *Journal of Applied Mechanics*, 24, 361.

[26] M. W. Barsoum, B. Cantor and M. J. Goringe (Eds.), (2003). Fundamentals of Ceramics (pp. 356-399). New York, NY: Taylor & Francis Group.

[27] ASTM C1322-05b, (2008). Standard Practice for Fractography and Characterization of Fracture Origins in Advanced Ceramics, *American Society for Testing and Materials*.

[28] K.T. Faber, and A.G. Evans, (1983). Crack deflection processes—I. Theory, *Acta Metallurgica*, 31(4), 565.

[29] R.W. Steinbrech, (1992). Toughening Mechanisms for ceramic materials, *Journal of the European Ceramic Society*, 10(3), 131.

[30] W. Kreher, (1992). On residual stresses in particle reinforced ceramics, *Journal of the European Ceramic Society*, 10(3), 167

[31] P.F. Becher, (1992). Microstructural Design of Toughened Ceramics, *Journal of the American Ceramic Society*, 74(2), 255.

[32] V. Tvergaard, (1992). Effect of ductile particle debonding during crack bridging in ceramics, *International Journal of Mechanical Sciences*, 34(8) 635.

[33] Z.Y. Deng, J. She, J.F. Yang, T. Ohji, and Y. Tanaka, (2004). Reinforcement by crack-tip blunting in porous ceramics, *Journal of the European Ceramic Society*, 24(7), 2055.

[34] S.N. Nasser, and L. Ni, (2001). A fiber-bridged crack with rate-dependent bridging forces, *Journal of the Mechanics and Physics of Solids*, 49(11), 2635.

[35] R. H. Hannink, P. M. Kelly, and B. C. Muddle, (2000). Transformation toughening in Zirconia containing ceramics, *Journal of the American Ceramic Society, 83*, 461.

[36] P. M. Kelly, and L. R. Francis Rose, (2002). The martensitic transformation in ceramics — its role in transformation toughening, *Progress in Materials Science, 47*(5), 463.

[37] B. Basu, (2004). Toughening of yttria-stabilised tetragonal zirconia ceramics, *Journal of the American ceramic society, 50(4),* 255.

[38] S. Shukla and S. Seal, (2005). Mechanisms of room temperature metastable tetragonal phase stabilisation in zirconia, *International Materials Reviews*. 50(1), 45.

[39] J. Chevalier, L. Gremillard, A. V. Virkar, and C. R. Clarke, (2009). The Tetragonal-Monoclinic Transformation in Zirconia: Lessons Learned and Future Trends. *Journal of the American Ceramic Society, 92(9),* 1901.

[40] B. Basu, J. Vleugela, and O. Van Der Biest, (2004). Transformation behavior of tetragonal zirconia: role of dopant content and distribution, *Materials Science and Engineering: A*, 336(2), 338.

[41] H.G. Scott, (1975). Phase relationships in the zirconia-yttria system, *Journal of Materials Science*, 10(9), 1527.

[42] N. Sneddon, (1946). The Distribution of Stress in the Neighborhood of a Crack in an Elastic Solid, Proceedings of the Royal Society A, 187(1009), 229.

[43] B. R. Lawn, E. R. Fuller, (1975). Equilibrium penny-like cracks in indentation fracture, *Journal of Materials Science,* 10, 2016.

[44] B. R. Lawn, E. R. Fuller, (1984). Measurement of thin-layer surface stresses by indentation fracture, *Journal of Materials Science*, 19(12), 4061.

[45] M.V. Swain, (2010). Unstable cracking (chipping) of veneering porcelain on all-ceramic dental crowns and fixed partial dentures, *Acta Biomaterialla*, 5(5), 2009.

[46] J.Y Thompson, K.J. Anusavice, A. Naman, and H.F. Morris, (1994). Fracture characterization of clinically failed all-ceramics crowns, *Journal of Dental Research*, 73(12), 1824.

[47] J. R. Kelly, J. A. Tesk, and J. A. Sorensen, (1995). Failure of all-ceramic fixed partial dentures in vitro and in vivo: Analysis and modeling, *Journal of Dental Research*, 74(6), 1253.

[48] B. Taskonak, J. J. Mecholsky, K. J. Anusavice, (2005). Residual Stresses in bilayer dental ceramics. *Biomaterials*. 26, 3235.

[49] E. D. Rekow, N. R. F. A. Silva, P. G. Coelho, Y. Zhang, P. Guess, and V. P. Thompson, (2011). Performance of Dental Ceramics--Challenges for Improvements. *Journal of Dental Research.* 90, 937.

[50] C.W. Fairhurst, P.E. Lockwood, R.D. Ringle, and W.O. Thompson, (1992). The effect of glaze on porcelain strength, *Dental Materials*, 8, 203.

[51] B. Dunn, M.N. Levy, and M.H. Riesbick, (1977). Improving fracture resistance of dental ceramic, *Journal of Dental Research*, 56(10), 1209.

[52] J. Shen, and D.J. Green, (2004). Prediction of stress profiles in ion exchanged glasses, *Journal of Non-Crystalline Solids*, 344, 79.

[53] M. Ohring, (2001). Materials Science of Thin Films (2nd Edition). Waltham, MA.

[54] J. A. Thornton, (1986). The microstructure of sputter-deposited coatings, *Journal of Vacuum Science and Technology A*, *6*, 3059.

[55] C. V. Thompson, (2000). Structure Evolution During Processing of Polycrystalline Films, *Annual Review of Materials Science, 30,* 159.

[56] J. R. Piascik, J. Y. Thompson, C. A. Bower, and B. R. Stoner, (2006). Stress evolution as a function of substrate bias in rf magnetron sputtered yttria-stabillized zirconia films, Journal of Vacuum Science and Technology 24, 1091.

[57] J. R. Piascik, Q. Zhang, C. A. Bower, J. Y. Thompson, and B. R. Stoner, (2007). Evidence of stress-induced tetragonal-to-monoclinic phase transformation during sputter deposition of YSZ, *Journal of Materials Research*, *22*, 1105.

[58] A. Misra, and M Nastasi, (1999). Evolution of tensile residual stress in thin metal films during energetic particle deposition, *Journal of Materials Research*, 14(12), 4466.

[59] Y.H. Wang, and X.P. Li, (1994). Phase Structure Characteristics of r.f. reactively sputtered zirconia thin film, *Thin Solid Films*, 250(1-2), 132.

[60] G.C.A.M. Jansen, M.M. Abdalla, F. van Keulen, B.R. Pujada, and B. van Venrooy, (2009). Celebrating the 100th anniversary of the stoney equation for film stress-developments from polycrystalline steel strips to single crystal silicon wafers, *Thin Solid Films*, 517(6) 1858.

[61] X. Feng, Y. Huang, and A.J. Rosakis, (2007). On the Stoney formula for a thin film/substrate system with nonuniform substrate thickness, *Journal of Applied Mechanics*, 74(6), 1276.

[62] ASTM C1499-09, (2009). Standard Test Method for Monotonic Equibiaxial Flexural Strength of Advanced Ceramics at Ambient Temperature, *American Society for Testing and Materials*.

[63] ASTM C1161-02c, (2008). Standard Test Method For Flexural Strength of Advanced ceramics at Ambient Temperature, *American Society for Testing and Materials*.

[65] J. T. DeMasi-Marcin, and D. K. Gupta, (1994). Protective Coatings in the Gas Turbine Engine, *Surface and Coatings Technology, 68,* 1.

[66] P. Y. Pekshev, S. V. Tcherniakov, N. A. Arzhakin, and V. V. Rutskin, (1994). Plasma-sprayed multilayer protective coatings for gas turbine units, *Surface and Coatings Technology, 64(1), 5.*

[67] A. I. Shaula, J. C. Oliveria, V. A. Kolotygin, C. Louro, V. V. Kharton, and A. Cavalerio, (2009). Protective YSZ-based thin films deposited by RF magnetron sputtering, *Vacuum*. 83(10), 1266.

[68] A. D. Bona, and R. Van Noort, (1995). Shear vs Tensile Bond Strength of Resin Composite Bonded to Ceramic, *Journal of Dental Research, 74,* 1591.

[69] I. Stangel, D Nathanson, and C. S. Hsu, (1987). Shear Strength of the Composite Bond to Etched Porcelain, *Journal of Dental Research, 66(9),* 1460.

[70] H. Assender, V. Bliznyuk, and K. Porfyrakis, (2002). How Surface Topography Relates to Materials' Properties, *Science 297(5583),* 973.

[71] T. Kosmac, C. Oblak, P. Jevnikar, N. Funduk, and L. Marion, (1999). The effect of surface grinding and sandblasting on flexural strength and reliability of Y-TZP zirconia ceramic, *Dental Materials*, *15*(6), 426.

[72] S. M. Wiederhorn, (1984). Brittle Fracture and Toughening Mechanisms in Ceramics, *Annual Reviews of Materials Science, 14,* 373.

[73] Z. Ji, J. A. Haynes, E. Voelkl, and J. M. Rigsbee, (2001). Phase Formation and Stability in Reactively Sputter Deposited Yttria-Stabilized Zirconia Coatings, *Journal of the American Ceramic Society*, 84(5), 929.

[74] T. S. Oh, J. Rödel, R. M. Cannon, and R. O. Ritchie, (1988). Ceramic-metal interfacial crack growth: Toughening by controlled microcracks and interfacial geometries, *Acta Metallurgica*, 36(8), 2083.

[75] A. Van Der Drift, (1967). Evolutionary Selection, a principle governing growth orientation in vapor-deposited layers, *Philips Research Reports*, 22, 267.

[76] C. V. Thompson, (1990). Grain Growth in Thin Films, *Annual Review of Materials Science*, 20, 245.

[77] C. V. Thompson, (1995). Texture development in polycrystalline thin films, *Materials Science and Engineering B*. 32(3), 211.

[78] B. Cales, and Y. Stefani, (1994). Mechanical properties and surface analysis of retrieved zirconia hip joint heads after an implantation of two to three years, *Journal of Materials Science: Materials in Medicine*, 5, 376.

[79] G. M. Loughran, A. Versluis, and W. H. Douglas. (2005), Evaluation of sub-critical fatigue crack propagation in a restorative composite, *Dental Materials*, 21(3) 252.

[80] J. R. Kelly, (1997). Ceramics in Restorative and Prosthetic Dentistry, *Annual Reviews of Materials Science*, 27, 443.

[81] K. J. Anusavice, (1992). Degradability of Dental Ceramics, *Advances in Dental Research,* 6, 82.

[82] M. Albakry, M. Guazzato, and M. V. Swain, (2004). Effect of sandblasting grinding polishing and glazing on the flexural strength of two pressable all-ceramic dental materials, *Journal of Dentistry*, 32(2), 91.

[83] M. J. Cattell, R. L. Clarke, and E. J. R. Lynch, (1997). The Biaxial Flexural Strength and Reliability of Four Dental Ceramics – Part II, *Journal of Dentistry,* 25(5), 409.

[84] R. L. Sakaguchi, M. Cross, and W. H. Douglas, (1992). A simple model of crack propagation in dental materials, *Dental Materials* 8(2), 131.

[85] M. N. Aboushelib, and H. Wang, (2010). Effect of Surface Treatment on Flexural Strength of Zirconia Bars, *Journal of Prosthetic Dentistry,* 104(2), 98.

[86] C. Piconi, and G. Maccauro, (1999). Zirconia as a Ceramic Biomaterial, *Biomaterials*, 20(1), 1.

[87] J. Chevalier, (2006). What Future For Zirconia As A Biomaterial, *Biomaterials*, 27(4), 535.

[88] J. Zhou, J. Mah, P. Shrotriya, C. Mercer, and W. O. Soboyejo, (2007). Contact damage in an yttria stabilized zirconia: Implications for biomedical applications, *Journal of Materials Science: Materials in Medicine* 18(1), 71.

[89] S. B. Amor, B. Rogier, G. Baud, M. Jacquet, and M. Nardin, (1998). Characterization of zirconia films deposited by r.f. magnetron sputtering, *Materials Science and Engineering: B*, 57(1), 28.

[90] M. Taira, Y. Nomura, K. Wakasa, M. Yamaki, and A. Matsui, (1990). Studies on fracture toughness of dental ceramics, *Journal of Oral Rehabilitation,* 17(6), 551.

[91] S. S. Scherrer, J. R. Kelly, G. D. Quinn, and K. Xu, (1999). Fracture toughness (K1c) of a dental porcelain determined by fractographic analysis, *Dental Materials*, 15(5), 342.

[92] R. R. Seghi, I. L. Denry, and S. F. Rosenstiel, (1995). Relative fracture toughness and hardness of new dental ceramics , *The Journal of Prosthetic Dentistry*, 74(2), 145.

[93] H. Yilmaz, C. Aydin, and B. E. Gul, (2007). Flexural Strength and Fracure Toughness of Dental Core Ceramics, *The Journal of Prosthetic Dentistry,* 98(2), 120.

[94] R. L. Smith, J. Y. Thompson, R. N. Chan, B. R. Stoner, J. R. Piascik, and J. J. Mecholsky, (2012). Triple Blind Fractography Study of Yttria-Stabilized Zirconia Thin-Film-Modified Porcelain, *Fractography of Glasses and Ceramics VI: Ceramic Transactions* 230, 265.

[95] O. Knotek, R. Elsing, G. Kramer, and F. Jungblut, (1991). On the origin of compressive stress in PVD coatings — an explicative model, *Surface and Coatings Technology*, 46(3), 265.

[96] M. Øilo and N.R. Gjerdet, (2013). Fractographic analyses of all-ceramic crowns: A study of 27 clinically fractured crowns, *Dental Materials*, 29(6), e78.

[97] H. Fischer and R. Marx, (2001). Improvement of Strength Parameters of a Leucite-reinforced Glass Ceramic by Dual-ion Exchange, *Journal of Dental Research*, 80(1), 336.

[98] I. Denry and J.A. Holloway, (2009). Ceramics for Dental Applications: A Review, *Materials*, 3(1), 351.

[99] M. Baldassarri, C.F. Stappert, M.S. Wolff, V.P. Thompson, and Y. Zhang, (2012). Residual Stresses in porcelain-veneered zirconia prostheses, *Dental Materials*, 28(8), 873.

[100] M.N. Aboushelib, A.J. Feilzer, and C.J. Kleverlaan, (2009). Bridging the gap between clinical failure and laboratory fracture strength tests using a fractographic approach, *Dental Materials*, 25(3), 383.

[101] B. Taskonak, J.A. Griggs, J.J. Mecholsky, and J. Yan, (2008). Analysis of subcritical crack growth in dental ceramics using fracture mechanics and fractography, *Dental Materials*, 24(5) 700.

[102] R. Tandon and R.E. Cook, (1993). Indentation Crack Initiation and Propagation in Tempered Glass, *Journal of the American Ceramic Society*, 76(4), 885.

[103] T.E. Buchheit and R. Tandon, (2007). Measuring Residual Stress in Glasses and Ceramics using Instrumented Indentation, *Journal of Materials Research*, 22(10), 2875.

[104] D.J. Green, R. Tandon, and V.M. Sglavo, (1995). Crack Arrest and multiple cracking in glass through the use of designed residual stress profiles, *Science*, 283(5406), 1295.

[105] B. Dunn, M.N. Levy, M.H. Riesbick, (1977). Improving the Fracture Resistance of Dental Ceramic, *Journal of Dental Research*, 56(10), 1209.

[106] R.N. Chan, B.R. Stoner, J.Y. Thompson, R.O. Scattergood, J.R. Piascik, (2013). Fracture toughness improvements of dental ceramic through use of yttria-stabilized zirconia (YSZ) thin-film coatings, Dental Materials, 29(8), 881.

[107] J.A. Thornton, and D.W. Hoffman, (1989). Stress-Related Effects in Thin Films, *Thin Solid Films*, 171(1), 5.

[108] W. Weibull, (1951), A Statistical Distribution Function of Wide Applicability, *Journal of Applied Mechanics*, 18, 293.

[109] A.V. Virkar, (1990). Determination of Residual stress profile using a strain gage technique, *Journal of the American Ceramic Society*, 73(7), 2100.